The Company of **Biologists**

RESEARCH ARTICLE

Regulation of anterior neurectoderm specification and differentiation by BMP signaling in ascidians

Agnès Roure, Rafath Chowdhury* and Sébastien Darras‡

ABSTRACT

The most anterior structure of the ascidian larva is made of three palps with sensory and adhesive functions essential for metamorphosis. They derive from the anterior neural border and their formation is regulated by FGF and Wnt. Given that they also share gene expression profiles with vertebrate anterior neural tissue and cranial placodes, their study should shed light on the emergence of the unique vertebrate telencephalon. We show that BMP signaling regulates two phases of palp formation in *Ciona intestinalis*. During gastrulation, the anterior neural border is specified in a domain of inactive BMP signaling, and activating BMP prevented its formation. During neurulation, BMP defines ventral palp identity and indirectly specifies the inter-papilla territory separating the ventral and dorsal palps. Finally, we show that BMP has similar functions in the ascidian *Phallusia mammillata*, for which we identified novel palp markers. Collectively, we provide a better molecular description of palp formation in ascidians that will be instrumental for comparative studies.

KEY WORDS: Palps, Ascidian, BMP, Anterior neural boundary, Placode, Peripheral nervous system

INTRODUCTION

Ascidians (or sea squirts) belong to a group of marine invertebrates, the tunicates, that is the sister group of vertebrates (Delsuc et al., 2006). This phylogenetic position, together with a stereotyped embryonic development with few cells, puts ascidians as interesting models for developmental biology and comparative approaches to address questions regarding chordate evolution and the emergence of vertebrates. Ascidians have a biphasic life cycle: following external development, the embryo gives rise to a swimming tadpole-like larva with typical chordate features (notochord, dorsal neural tube) that then attaches to a substrate before metamorphosing into a sessile adult ascidian with a radically different body plan, a 'bag' with two siphons. Metamorphosis is controlled by a specific organ, the palps (also referred to as the adhesive organ or the adhesive papillae), which is located at the anterior end of the larva. The palps are a specialized part of the ectoderm that has adhesive and sensory properties (Cloney, 1977; Imai and Meinertzhagen, 2007; Satoh, 1994). They enable the larva to select a suitable substrate for metamorphosis, via a chemo- and/or mechano-sensory function, and to attach to it through the secretion of adhesive materials

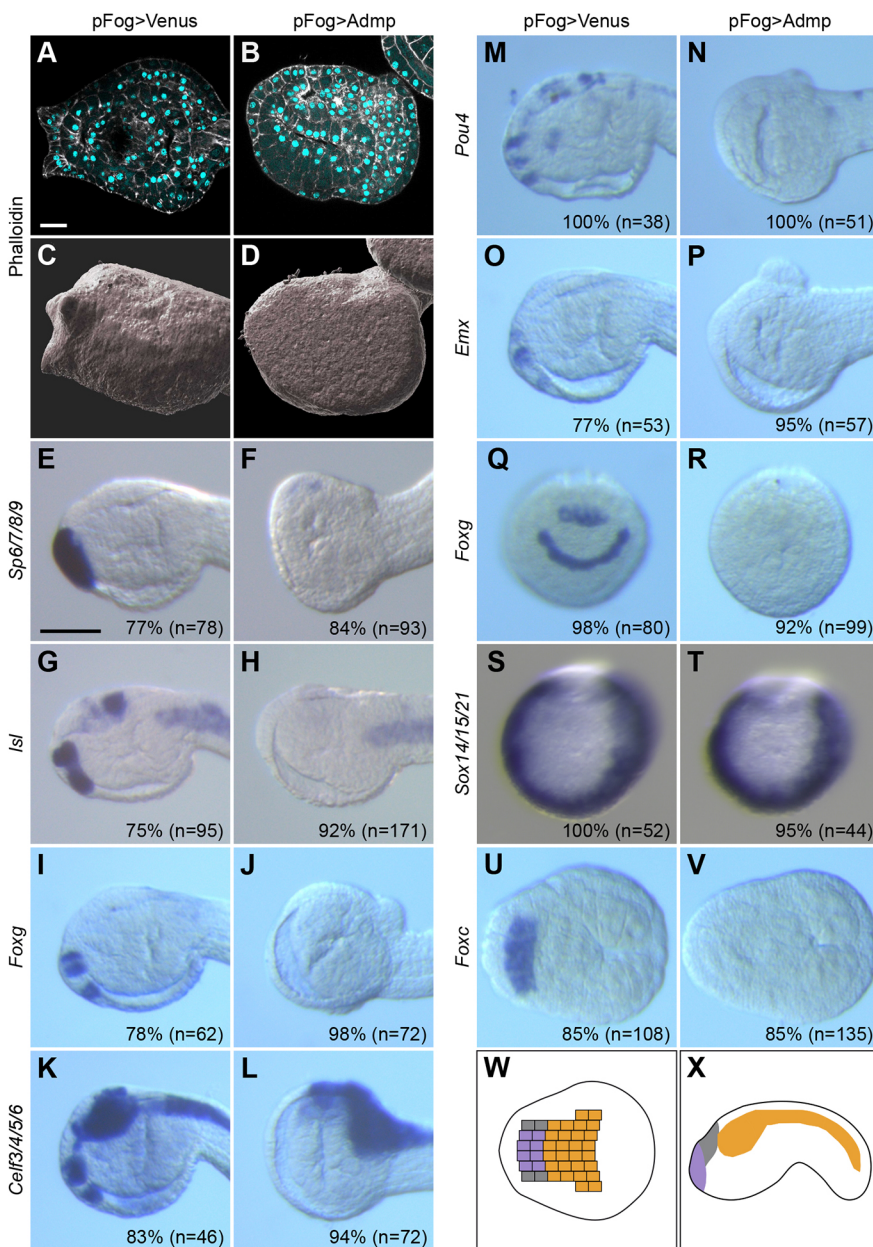Sorbonne Université, CNRS, Biologie Intégrative des Organismes Marins (BIOM), F-66650, Banyuls/Mer, France.
*Present address: Departament de Genètica, Microbiologia i Estadistica, Facultat de Biologia, Universitat de Barcelona, Spain.

‡Author for correspondence (sebastien.darras@obs-banyuls.fr)

S.D., 0000-0002-0590-0062

(reviewed by Pennati and Rothbächer, 2015). The palps contain at least four cells types for which the specification and function have not yet been deciphered in detail (Johnson et al., 2020; Zeng et al., 2019). Three cell types – the ciliated sensory neurons, the collocytes (containing vesicles filled with adhesive material) and the axial columnar cells (ACCs) (myoepithelial cells controlling palp retraction following adhesion) – are elongated cells forming a protrusion. Three protrusions or papillae (two dorsal papillae that are bilaterally symmetrical, and a ventral papilla located at the midline; Fig. 1C) make up the palps and are separated by the fourth cell type, the non-elongated inter-papillae cells.

Palps belong to the peripheral nervous system and studies of palps have been instrumental in the proposal of evolutionary scenarios relating to the nervous system in chordates (Cao et al., 2019; Horie et al., 2018; Poncelet and Shimeld, 2020; Thawani and Groves, 2020). In the ascidian *Ciona intestinalis*, palp cell lineage and topology, together with gene expression data and functional studies, have shown to have similarities to anterior derivatives of the vertebrate nervous system, the olfactory placodes and the telencephalon (Cao et al., 2019; Horie et al., 2018; Hudson et al., 2003; Liu and Satou, 2019; Poncelet and Shimeld, 2020; Thawani and Groves, 2020; Wagner and Levine, 2012; Wagner et al., 2014). Palps originate from precursors that are located at the anterior edge of the neural plate during gastrulation, which we will refer to as the anterior neural border (ANB) (Fig. 1W,X) (Horie et al., 2018; Liu and Satou, 2019). Although the ANB is not part of the central nervous system (CNS), it originates from the same lineage specified by fibroblast growth factor (FGF)-mediated neural induction at the 32-cell stage and expresses neural markers such as *Celf3/4/5/6* (also known as *Etr* and *Celf3.a*) and *Otx* (Horie et al., 2018; Hudson, 2016; Hudson et al., 2003; Nishida, 1987). The separation between these two lineages is regulated by FGF/Erk signaling at gastrula/neurula stages, FGF being active in the CNS precursors (Hudson, 2016; Hudson et al., 2003; Wagner and Levine, 2012). FGF signaling thus regulates positively and negatively two separate phases of palp specification. The ANB also expresses *Dmrt* and *Foxc*, coding for transcription factors that are essential for palp formation (Imai et al., 2006; Wagner and Levine, 2012). From neurulation and through differentiation, palps express genes such as *Dlx.c*, *Foxg*, *Isl* or *Sp6/7/8/9* (also known as *Zf220* and *Btd*) orthologs of which specify anterior neural territories and placodes in vertebrates (Cao et al., 2019; Liu and Satou, 2019; Wagner et al., 2014). In particular, *Foxg* and *Isl* are essential for palp formation (Liu and Satou, 2019; Wagner et al., 2014). The ANB thus shares similarities with vertebrate anterior cranial placodes, and the palps share similarities with derivatives of the vertebrate telencephalon, such as the olfactory bulb, and of the anterior placodes. It has been proposed that co-option of ANB/palp gene network to the anterior CNS led to the emergence of the vertebrate telencephalon (Cao et al., 2019).

Although knowledge of transcription factor functions and interactions in palp formation has been elucidated in some detail (Horie et al., 2018;

DEVELOPMENT

1

Fig. 1. Early BMP activation prevents palp formation. The BMP pathway was activated by overexpressing the BMP ligand Admp using the *Fog* ectodermal promoter. Experimental embryos were compared with control (overexpressing the fluorescent protein Venus). (A-D) Papilla protrusions and elongated cells were absent following BMP activation as revealed by confocal stacks for phalloidin (white) and DAPI (cyan) staining at larval stages (A,B: confocal sections; C,D: surface rendering). Scale bar: 20 μm. (E-V) BMP activation repressed genes expressed in the palps as determined by *in situ* hybridization for *Sp6/7/8/9* (E,F), *Isl* (G,H), *Foxg* (I,J), *Celf3/4/5/6* (K,L), *Pou4* (M,N) and *Emx* (O,P) at mid-tailbud stages (St. 23), and *Foxg* (Q,R) and *Foxc* (U,V) at neurula stages. The expression of the epidermis marker *Sox14/15/ 21*, which is excluded from the palps at neurula stages, was unchanged (S,T). For each panel, n indicates the number of embryos examined. The percentages correspond to normal expression for pFog>Venus, and to gene repression (except for *Sox14/15/21*) in the palp territory for pFog>Admp. Experiments were performed at least twice, except for *Celf3/4/5/6*, *Pou4*, *Emx* and *Sox14/15/21* for which results come from a single experiment. In tailbud embryos, a bulging mass of cells was often visible in the dorsal posterior trunk. It most likely corresponds to the CNS as revealed by *Celf3/4/5/6* expression, which was detected outside of the embryo owing to abnormal neural tube closure. Anterior is to the left in lateral views except Q-T (frontal views) and U,V (neural plate views). Scale bar: 50 μm. (W,X) Schematics of the progeny of the neural plate. Orange, CNS; purple, palp region; gray aATENS (sensory neurons of the trunk PNS) precursors (adapted from Horie et al., 2018; Liu and Satou, 2019).

Liu and Satou, 2019; Wagner et al., 2014), the role of cell–cell communication is scarce except for the involvement of FGF/Erk pathway (Hudson et al., 2003; Wagner and Levine, 2012). We have previously shown that inhibition of canonical Wnt pathway is essential for ANB specification (Feinberg et al., 2019), but an understanding of the role of Wnt signaling later in development is still lacking. In a distantly related ascidian species, *Halocynthia roretzi*, morphological data indicate that activating the BMP pathway abolishes palp formation whereas BMP inhibition results in palps made of a single protrusion instead of three (Darras and Nishida, 2001), but the lack of molecular analysis prevents us from precisely determining the function of BMP signaling.

We have directly addressed the function of BMP signaling pathway in palp formation during embryogenesis of the ascidian *C. intestinalis*. We show that BMP is involved in two consecutive phases. Up to neurulation, ANB specification is incompatible with active BMP signaling, and the ANB forms in a region devoid of active BMP (as revealed by phospho-Smad1/5/8 immunostaining). Consequently, early activation of BMP prevents palp formation

through the inhibition of ANB precursor formation. Following gastrulation, BMP participates in the differentiation of the palps through the specification of the ventral papilla and the regulation of the papillae versus inter-papillae fate decision. In particular, BMP-inhibited larvae harbor a single, large protrusion made of elongated cells, the *Cyrano* phenotype, with an increased number of sensory neurons and ACCs. We propose that the competence to become a papilla is regulated by BMP through the transcription factor-coding genes *Foxg* and *Sp6/7/8/9*. Interestingly, we show that modulating BMP pathway in the ascidian *Phallusia mammillata* (275 My of divergence time) produces the same phenotypes as in *C. intestinalis*. This allowed us to use previously published RNA-seq data (Chowdhury et al., 2022) to identify a number of genes expressed in the ANB and the palps. Altogether, our work points to a role for signaling pathway inhibition in ANB specification, similar to early anterior neurectoderm formation in vertebrates. Moreover, we provide a significant contribution to knowledge of the palp gene network, an essential requisite to probing its conservation with the

networks regulating cranial placodes and telencephalon formation in vertebrates.

RESULTS
BMP activation abolishes palp formation
When we activated the BMP signaling pathway by overexpressing, in the ectoderm, the BMP ligand Admp by electroporation using the pFog driver (active from the 16-cell stage) (Pasini et al., 2006; Rothbacher et al., 2007), we observed an absence of protrusions that are obvious features of the adhesive palps. The anterior end of the larvae were smooth, and epidermal cells were flat and did not display the typical elongated shape (Fig. 1A-D). This morphological evidence was accompanied by repression of the expression at mid-tailbud stages of all the genes expressed in the palps that we examined: *Sp6/7/8/9*, *Isl*, *Foxg*, *Celf3/4/5/6*, *Pou4* and *Emx* (Fig. 1E-P). Palps derive from the median ANB at gastrula stages (Fig. 1W,X) and can be tracked by the expression of genes essential for palp formation, *Foxg* at neurula stages (Fig. 1Q,R) and *Foxc* at gastrula stages (Fig. 1U,V) (Liu and Satou, 2019; Wagner and Levine, 2012). Both genes were repressed by BMP activation, and this repression is sufficient to explain the later lack of palp gene expression and differentiation. Interestingly, palps were not converted into general epidermis as the epidermal marker *Sox14/15/21* (also known as *SoxB2*) was normally expressed and did not show ectopic expression in the palp area (Fig. 1S,T).

Dynamic BMP activity in the palp-forming region
The above results suggest that active BMP signaling is incompatible with palp formation. Active BMP signaling can be determined by examining the phosphorylated (active) form of the BMP transducer Smad1/5/8. It has been previously shown that BMP is active from late gastrula to early tailbud stages in the ventral epidermis midline of *Ciona robusta* embryos (Waki et al., 2015). We obtained similar results in *C. intestinalis* using a different antibody (Fig. 2). More specifically, up to gastrulation, we did not detect significant levels for P-Smad1/5/8 except in a few posterior endomesodermal cells (Fig. 2A). At mid-gastrula, P-Smad1/5/8 was present in the nuclei of the posterior (b-line) ventral midline epidermis (Fig. 2B). Consequently, at the onset of *Foxc* expression in palp precursors (St. 10), BMP was not active in the palp-forming region (Fig. 2L). Shortly after, at early neurula stages, P-Smad1/5/8 extended into the anterior (a-line) ventral midline epidermis (Fig. 2C). During neurulation, the posterior limit of P-Smad1/5/8 gradually shifted anteriorly, in agreement with the dynamic posterior-to-anterior expression of candidate target genes (Roure and Darras, 2016); by mid-tailbud stages, P-Smad1/5/8 was restricted to the trunk ventral epidermis (Fig. 2D,E,J). In addition, active Smad1/5/8 was also detected in the endoderm underlying the ventral epidermis midline with a similar temporal dynamic (Fig. 2E,F,H,J,K), and in a group of cells of the anterior sensory vesicle at mid-tailbud stages (Fig. 2E,J, K). We validated the specificity of these results by modulating the BMP pathway: when embryos were treated with BMP2 protein, P-Smad1/5/8 was ectopically detected in the entire epidermis at early neurula stages, whereas no staining was observed following inhibition using the pharmacological inhibitor DMH1 (Fig. S1).

To relate precisely the location of active signaling in the ectoderm and palp precursors, we performed double staining: P-Smad1/5/8 immunostaining and *in situ* hybridization for the early palp markers *Foxc* and *Foxg* (Fig. 2F-J). At late gastrula stages, P-Smad1/5/8 abutted *Foxc* expression domain, confirming that palp precursors were specified in a BMP-negative domain (Fig. 2F,G,L). Later, we observed P-Smad1/5/8 in the median *Foxc* expression domain at mid neurula stages (not shown) and in the median part of the U-shaped *Foxg* expression domain

in late neurulae (Fig. 2H,I,L), corresponding presumably to the future ventral palp. This was confirmed by co-expression of P-Smad1/5/8 and *Foxg* in ventral cells of early tailbuds (Fig. 2J-L). In summary (Fig. 2K, L), BMP signaling was absent from the ANB (marked by *Foxc*) until the early neurula stages; active BMP signaling was detected from mid neurula stages in the future protrusion (*Foxg*$^+$ cells) of the ventral palp.

BMP inhibition participates in ANB definition
We next tested whether BMP inhibition was sufficient to induce an ANB fate. When BMP signaling was blocked either by overexpression of the secreted inhibitor Noggin or by treatment with the BMP receptor inhibitor DMH1, *Foxc* expression at late gastrula stages was unchanged (Fig. 3A-C). The fact that *Foxc* was not ectopically expressed following BMP inhibition could be explained by an incomplete BMP blockade. However, DMH1 treatment led to undetectable P-Smad1/5/8 levels (Fig. S1). Alternatively, it could be that the number of cells that are competent to become ANB in response to BMP inhibition could be restricted to the cells already expressing *Foxc*. *Foxc* expression and palp fate are regulated by FGF signaling following neural induction and cell fate segregation (Wagner and Levine, 2012). We thus aimed at increasing the number of cells competent to form ANB by early activation of FGF signaling using treatment with recombinant bFGF protein, and testing the effects of BMP pathway modulations in this context. As expected, bFGF treatment from the 8-cell stage neuralized the entire ectoderm, as revealed by the ectopic expression of the neural markers *Otx* and *Celf3/4/5/6* and the downregulation of the epidermal marker *Tfap2-r.b* (also known as *Ap2-like2*) at late gastrula stages [(Fig. 3Div-Fiv,Hiv) when compared with control embryos (Fig. 3Di-Fi,Hi)]. The effects of FGF were not modified by activation (Fig. 3Dv-Fv,Hv) or inhibition (Fig. 3Dvi-Fvi,Hvi). *Foxc* behaved somewhat unexpectedly: it was either ectopically expressed in a fraction of the embryos (53%, *n*=69; Fig. 3Giv) or repressed in the others (38%, *n*=69; not shown) when compared with ANB expression in controls (Fig. 3Gi). The repression of *Foxc* might be explained by the fact that FGF/Erk is downregulated in the palp lineage during gastrulation (Wagner and Levine, 2012), hence our continuous treatment might inhibit *Foxc* expression. Nevertheless, when the BMP pathway was inhibited on top of FGF activation, *Foxc* was strongly expressed, in all embryos, as a cup covering the anterior end including the ventral epidermis (Fig. 3Gvi). In addition, FGF activation did not overcome BMP-induced loss of Foxc expression (Fig. 3Gv). Our observations demonstrate that *Foxc* expression and ANB formation can only occur in a domain devoid of active BMP signaling.

Importantly, the loss of *Foxc* following BMP activation using recombinant BMP2 protein treatment was specific to this gene and did not result from neural tissue inhibition, as in vertebrates, because the neural markers *Otx* and *Celf3/4/5/6* were still expressed in the CNS but downregulated in the ANB (Fig. 3Dii,Eii,Hii). Reciprocally, BMP inhibition was not sufficient to lead to ectopic neural tissue formation (Fig. 3Diii-Hiii). This is in agreement with similar data produced in the distantly related ascidian *H. roretzi* (Darras and Nishida, 2001). Interestingly, although *Foxc* and *Tfap2-r.b* were co-expressed in the ANB, only *Foxc* was repressed by BMP (Fig. 3Fi,Fii,Gi,Gii and Fig. S2). However, because the ANB does not convert into epidermis (Fig. 1), it is likely that, although inhibiting palp fate, BMP signaling does not abolish all the effects of the induction by FGF.

The BMP signaling pathway regulates palp formation after ANB is specified
We examined whether modulating BMP had any impact on palp formation besides ANB specification. We thus performed
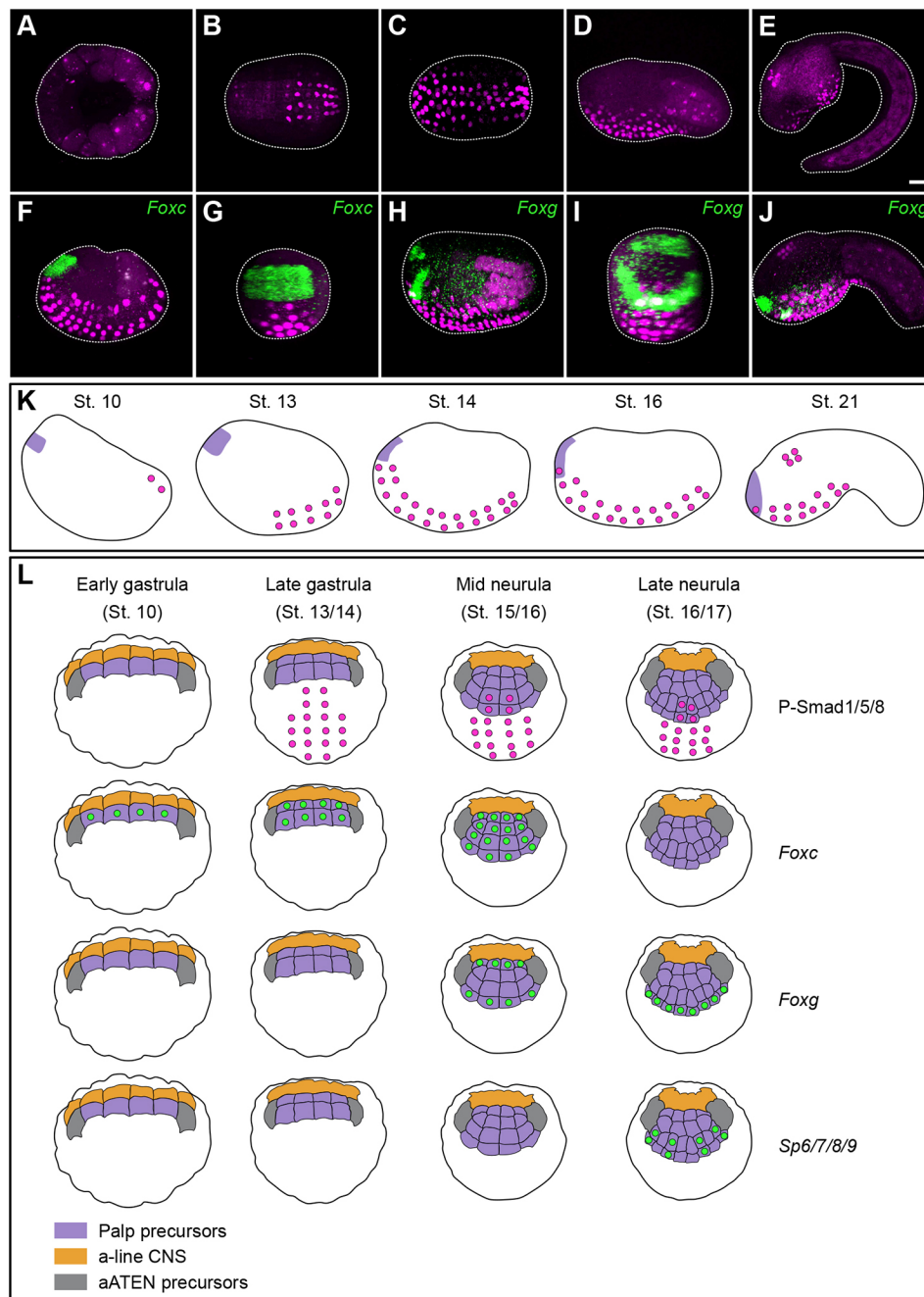
Fig. 2. Dynamic BMP activity in the palp-forming region. (A-E) P-Smad1/5/8 immunostaining (magenta) at various developmental stages in control embryos: (A) early gastrula (St. 11, vegetal view), (B) late gastrula (St. 13, ventral view), (C) neurula (St. 14/15, ventral view), (D) initial tailbud (St. 18, lateral view) and (E) late tailbud (St. 23, lateral view) stages. (F-J) P-Smad1/5/8 immunostaining (magenta) and in situ hybridization (green) for *Foxc* at early neurula stages (St. 14) (F,G), and *Foxg* at late neurula (St. 16) (H,I) and mid tailbud (St. 21) (J) stages of control embryos. Dorsal is to the top with lateral views and anterior to the left (F,H,J), or frontal views (G,I). F and G are different views of the same embryo. H and I are different views of another embryo. All data were obtained from at least two independent experiments. Scale bar: 20 µm. Embryos are outlined with white dotted lines. (K) Schematics of the dynamics of P-Smad1/5/8 (magenta circles) with respect to the palp-forming region (purple). The schemes depict sagittal sections with anterior to the left and dorsal to the top at early gastrula (St. 10/11), late gastrula (St.13), early neurula (St. 14), late neurula (St. 16) and mid tailbud (St. 21) stages. Main sites of expression are depicted: a few endomesodermal cells (St. 10/11), posterior ventral epidermis and endoderm (St. 13), ventral epidermis and endoderm throughout the antero-posterior axis (St. 14 and 16), ventral part of the palp-forming region (St. 16 and 21), trunk ventral epidermis, endoderm and sensory vesicle (St. 21). (L) Active BMP signaling (P-Smad1/5/8 in magenta) and palp gene expression (green) for *Foxc*, *Foxg* and *Sp6/7/8/9* were mapped onto schematic embryos according to the above data and previous reports (Horie et al., 2018; Liu and Satou, 2019). Schemes and lineages representing the frontal view of embryos during gastrulation and neurulation were drawn following *Phallusia mammillata* 4D reconstructions available at https://morphonet.org/ (Guignard et al., 2020; Leggio et al., 2019).

whole-embryo treatments starting at progressively later stages of embryonic development and examined the early marker *Foxc* and the late marker *Isl* (Fig. 4).

Activating BMP at early gastrula stages (St. 10) partially repressed *Foxc* whereas mid-gastrula (St. 12) treatment had no effect (Fig. 4). The time-dependent effects of BMP activation coincided with the dynamics of *Foxc* expression: before it was expressed (8-cell stage), the repression was complete (Fig. 3Gii); at the onset of expression (St. 10), the repression was milder; and once *Foxc* was robustly expressed (St. 12), there was no repression (Fig. 4). This is further supported by the fact that BMP2 treatment led to fast P-Smad1/5/8 nuclear accumulation (the shortest treatment we tested was 30 min; Fig. S1). The ventral spot of *Isl* expression was lost for treatments starting at St. 10 and St. 12, whereas later treatments did not change *Isl* expression (Fig. 4).

Inhibiting BMP had no effect on *Foxc* expression, similarly to the earliest treatment (Fig. 3Giii). *Isl*, which is normally expressed as three spots, had a U-shaped expression (Fig. 4). The same effect was observed by overexpressing Noggin using electroporation (Fig. S3). This phenotype was much less frequent when the DMH1 treatment started at late neurula stages (St. 16).

The changes in *Isl* expression prompted us to determine how palps differentiate when BMP is modulated from gastrula stages.

## A single protrusion with additional neurons following BMP inhibition

In DMH1-treated embryos, whereas *Isl* was expressed in the shape of a large U at mid-tailbud stages (St. 23) (Fig. 4), it was concentrated in a protruding structure at the anterior tip at late tailbud stages (St. 25) (Fig. 5E) when it was expressed in each of the
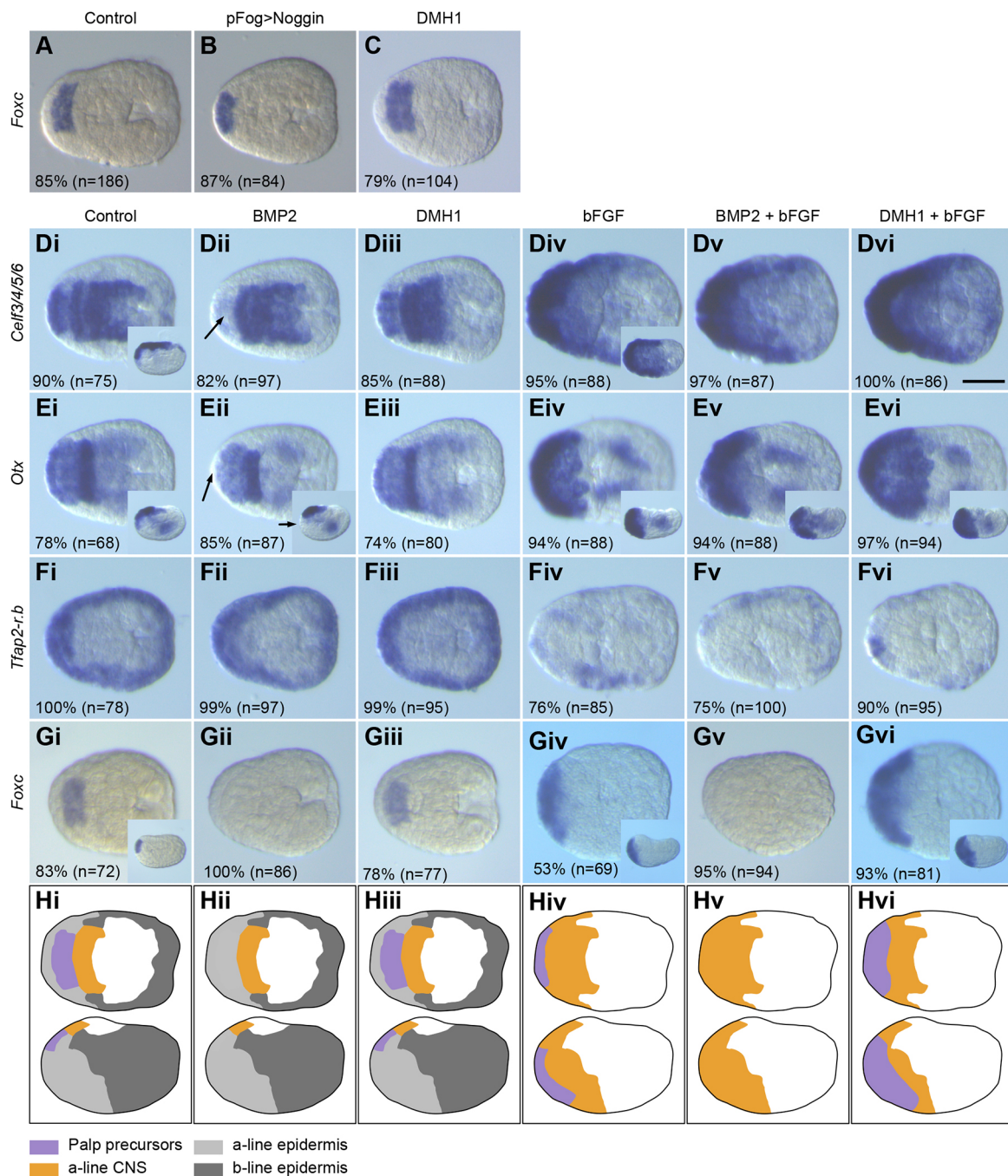
Fig. 3. Inactive BMP signaling is required for ANB specification. (A-C) *Foxc* expression by *in situ* hybridization at early neurula stages (St. 14) was unchanged following BMP pathway inhibition by Noggin overexpression (B) or DMH1 treatment from the 8-cell stage (C). (D-G) Embryos were treated from the 8-cell stage to fixation at early neurula stages (St. 14) with BMP2 protein or DMH1 alone, or in combination with bFGF protein. Gene expression was assessed by *in situ* hybridization for *Celf3/4/5/6* (Di-Dvi), *Otx* (Ei-Evi), *Tfap2-r.b* (Fi-Fvi) and *Foxc* (Gi-Gvi). For each panel, n indicates the number of embryos examined. The percentages indicate the frequency of the phenotype depicted in the picture. The results come from two independent experiments. Embryos are shown with anterior to the left in neural plate views except insets, which are lateral views with dorsal to the top. The arrows in Dii and Eii mark the downregulation of *Celf3/4/5/6* and *Otx* in the palp precursors. Scale bar: 50 µm. (H) Schematic interpretations of the consequences of the various treatments (i, control; ii, BMP2; iii, DMH1; iv, bFGF; v, BMP2+bFGF; vi, DMH1+bFGF) on some ectodermal derivatives: palp precursors (purple), a-line neural tissue (orange), a-line epidermis (light gray) and b-line epidermis (dark gray). The embryo schemes show a neural plate view (top) and a lateral view (bottom) with anterior to the left. The schemes were drawn using *Phallusia mammillata* 4D reconstructions available at https://morphonet.org/ (Guignard et al., 2020; Leggio et al., 2019).

three protrusions of the control embryos (Fig. 5A). In larvae, this single, large protrusion was made of elongated cells as visualized by phalloidin staining (Fig. 5F-H), similar to what was observed in each of the three papillae of control larvae (Fig. 5B-D). We coined

this phenotype *Cyrano* (in memory of the famous character depicted by Edmond Rostand). In *Ciona*, it is thought that palps contain a fixed number of the different cell types (Zeng et al., 2019). We performed fluorescence *in situ* hybridization at the late-tailbud stage
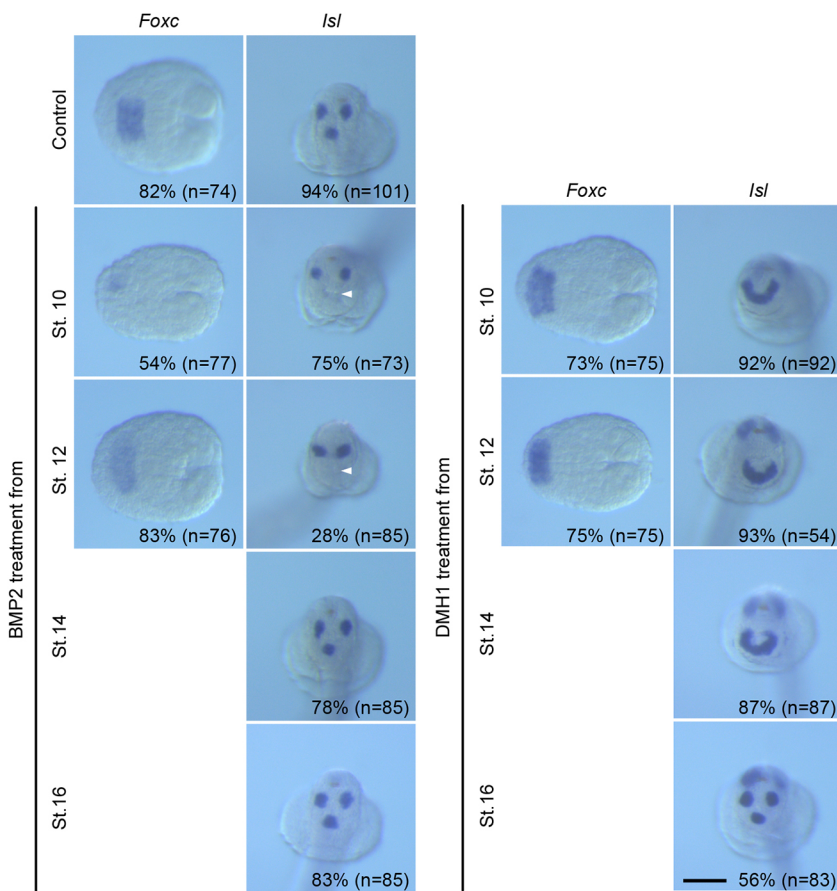
Fig. 4. Late effects of BMP pathway modulations on palp formation. Embryos were treated with BMP2 protein (left) or DMH1 (right) from the stage indicated on the figure up to fixation and *in situ* hybridization for *Foxc* at early neurula stages (St. 14) and *Isl* at late tailbud stages (St. 23). For each panel, n indicates the number of embryos examined. The percentages indicate the frequency of the phenotype depicted in the picture. The results come from two or more independent experiments. Embryos are shown in neural plate views with anterior to the left for *Foxc* and frontal view with dorsal to the top for *Isl*. White arrowheads highlight the absence of the ventral spot of *Isl*. Scale bar: 50 µm.

(St. 23) using four genes and made 3D reconstruction of the *z*-stacks acquired by confocal microscopy (see Materials and Methods) in order to determine the differentiation of the palps in the *Cyrano* embryos. In agreement with previous reports, we found that the ACC marker *Isl* was expressed in 12 cells in control embryos (four cells per papilla) (Fig. 5I,J,Q). By contrast, we found that the sensory neuron marker *Pou4* was expressed in ten cells instead of 12 (Fig. 5I,J,Q). Interestingly, both dorsal palps had four cells that surrounded the *Isl*-positive cells whereas the ventral palp contained two *Pou4*-positive cells located dorsally to the *Isl*-positive cells. In DMH1-treated embryos, the number of neurons increased to 18 on average and the number of ACCs to 18 (Fig. 5Q). The increase of *Celf3/4/5/6* cells was not statistically significant. Interestingly, the number of cells expressing *Sp6/7/8/9*, which has been described as an inter-papillae marker (Wagner et al., 2014), was decreased in DMH1-treated embryos (Fig. 5Q). These data are in agreement with the interpretation that the number of cells with papilla fate has increased, but their physical proximity likely leads to the formation of a single protrusion.

In DMH1-treated embryos, *Pou4* was expressed all around the *Isl* cells, like in the dorsal palps (Fig. 5M,N). This suggested that the *Cyrano* protrusion may have a dorsal identity. In support of this interpretation, we found that expression of the homeobox transcription factor *Msx*, which we found transiently expressed in the future ventral palp at the onset of *Isl* expression (Fig. 5K,L), was lost following BMP inhibition (Fig. 5O,P). Although we have performed a detailed analysis of the *Cyrano* phenotype only on embryos generated by DMH1 treatment starting at gastrula stages, a similar phenotype was observed upon Noggin overexpression (a single protrusion visualized by phalloidin staining in Fig. 5F;

U-shape/ectopic expression of *Isl* and *Celf3/4/5/6* in Fig. S3). In *Cyrano* embryos, the ventral palp is missing, the number of inter-palp cells is reduced, and there is an excess of dorsal protruding cells. This suggests that BMP is required to specify the ventral palp and inter-palp cells. When this pathway was inhibited, cells that have lost these fates would adopt a 'default' dorsal palp fate.

The ventral palp is missing following BMP activation
As expected from the *Isl* profile (Fig. 4), only two protruding papillae made of elongated cells developed dorsally in BMP2-treated embryos (Fig. 6G,H). They were similar to the papillae of control larvae (Fig. 6A,B). This morphological absence of ventral palp was only partially confirmed at the molecular level. Similarly to *Isl*, *Msx* expression was abolished in treated embryos, but the expression of *Pou4* revealed that one or two neurons were still present (Fig. 6C,D,I,J). *Sp6/7/8/9* was repressed in its most ventral expression domain (Fig. 6E,K). In conclusion, although the ventral protrusion is absent, palp identity is not completely suppressed. Accordingly, we did not detect ectopic expression of the epidermal gene *Sox14/15/21* (Fig. 6L) as its expression was similar in control embryos (Fig. 6F).

Although BMP is required to define ventral palp fate (Fig. 5), BMP activation neither leads to ectopic ventral palp formation nor ventralizes the dorsal palps (we did not detect obvious defects in dorsal palp differentiation, and we identified four *Pou4*+ cells surrounding *Isl*+ cells as in controls; Fig. 6C,I). Given that BMP suppresses ventral palp, it is likely that excessive or precocious BMP signaling levels are responsible for this phenotype.
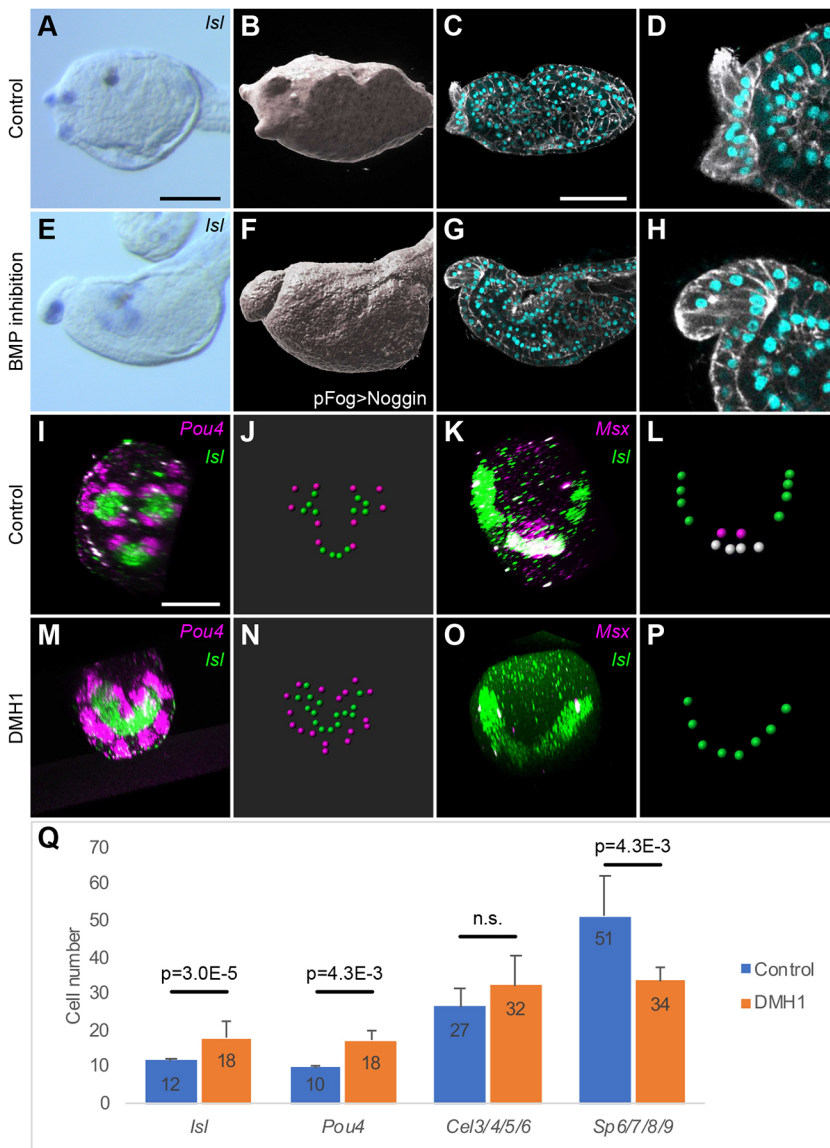
Fig. 5. BMP inhibition leads to the formation of a single large palp of dorsal character. (A-P) Embryos in which BMP signaling was inhibited in response to treatment with DMH1 from St. 10 (E,G,H,M-P) or Noggin overexpression (F) were compared with control embryos (A-D,I-L) for morphology and gene expression by *in situ* hybridization. *Isl*, normally expressed in each of the three protruding palps (A; 86%, *n*=7), was expressed as a large spot in a single protrusion at late tailbud stages (St. 25) in treated embryos (E; 100%, *n*=21). The single large protrusion is made of elongated cells (F-H; DAPI in cyan and phalloidin in white). (I,J,M,N) Double fluorescence *in situ* hybridization for *Pou4* (magenta) and *Isl* (green) in control (I) and treated (M) embryos at late tailbud stages (St. 23) with 3D representations of nuclei for cells expressing each gene (J,N). (K,L,O,P) Double fluorescence *in situ* hybridization for *Msx* (magenta) and *Isl* (green) in control (K) and treated (O) embryos at early tailbud stages (St. 19) with 3D representations of nuclei for cells expressing each gene (L,P). Co-expression of *Isl* and *Msx* appears white. Embryos are shown with dorsal to the top in lateral views (A-H) or frontal views (I-P). Scale bars: 50 µm (A-C,E-G,I-P); 20 µm (D,H). (Q) Quantification of the number of cells expressing each gene at late tailbud stages (St. 23) using 3D reconstructions as in J and N. The graph represents the average values from two or more independent experiments, with error bars denoting s.d. Differences in cell number were evaluated using the Mann–Whitney *U*-test, and *P*-values are indicated. n.s., not statistically significant. The numbers of embryos examined were as follows: control embryos (*Isl*, 14; *Pou4*, 5; *Celf3/4/5/6*, 5; *Sp6/7/8/9*, 6) and DMH1-treated embryos (*Isl*, 9; *Pou4*, 6; *Celf3/4/5/6*, 5; *Sp6/7/8/9*, 5).

BMP controls ventral palp and inter-palp fates through *Sp6/7/8/9* regulation

The U-shape pattern of *Isl* in DMH1 embryos reminded us of endogenous *Foxg* expression (Liu and Satou, 2019): at neurula stages, *Foxg* was expressed in the future palps following a U-shape that gradually converted into a three-spot pattern at tailbud stages that prefigures the three papillae protrusions (Fig. 7A-D). It thus seems that inhibiting BMP prevented the refinement of *Foxg* expression. Accordingly, *Foxg* expression was U-shaped following DMH1 treatment (Fig. 7E). Interestingly, knockdown of the zinc finger transcription factor-coding gene *Sp6/7/8/9* leads to a U-shaped *Foxg* expression (Liu and Satou, 2019). Because *Sp6/7/8/9* and *Foxg* are initially partially co-expressed before showing exclusive patterns (Fig. 2L), it has been proposed that *Foxg* restriction to the future protrusions is the result of repression by Sp6/7/8/9. We thus determined *Sp6/7/8/9* and *Foxg* expression following BMP modulation from early gastrula stages (Fig. 7). Although we confirmed initial co-expression using double-fluorescence *in situ* hybridization, we failed to obtain robust simultaneous expression allowing analysis the effects of the treatments (not shown). At St. 15/16, the onset of *Sp6/7/8/9* expression, *Sp6/7/8/9* was barely detectable

(Fig. 7F), and at St. 18/19, when *Sp6/7/8/9* expression was strong (Fig. 7G), *Foxg* showed a transient downregulation (Fig. 7B). We thus analyzed each gene at different stages [*Foxg* at late neurula stages (St. 16) (Fig. 7I-K) and *Sp6/7/8/9* at initial tailbud stages (St. 18) (Fig. 7L-N)]. When embryos were treated with BMP2 protein, the ventral expression of *Foxg* in the U-shape was missing (Fig. 7J) and *Sp6/7/8/9* was ectopically expressed at this location (Fig. 7M). Reciprocally, following DMH1 treatment, *Foxg* was unchanged (Fig. 7K) and ventral *Sp6/7/8/9* expression was shifted to a median position (Fig. 7N). Hence, *Sp6/7/8/9* was no more expressed in the ventral part of the U-shaped, palp-forming row of cells (Fig. 7T). We have summarized our understanding of these results in embryo schematics (Fig. 7O-T). Interestingly, DMH1 treatment had limited effects on *Isl* expression at St. 16 (Fig. 4), a timing that coincides with the onset of *Sp6/7/8/9* expression (Figs 2N and 7F).

Our results indicate that *Sp6/7/8/9* is positively regulated by BMP signaling. However, because it is not expressed in P-Smad1/5/8^{+} cells (Fig. 2L), we propose that an intermediate, yet unidentified, factor activates *Sp6/7/8/9* downstream of BMP in the neighboring cells (Fig. 7U,V). This hypothetical model of gene interaction is sufficient to explain *Sp6/7/8/9* and *Foxg* expression patterns and
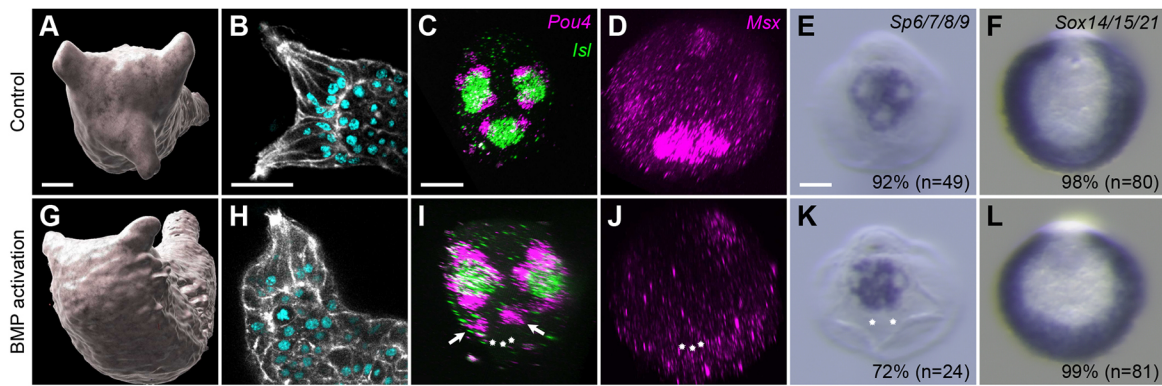
Fig. 6. Late BMP activation prevents ventral palp formation. (A-L) Embryos for which BMP signaling was activated by BMP2 treatment from St. 10 (G-L) were compared with control embryos (A-F) for morphology and gene expression by *in situ* hybridization. Whereas three protruding papillae made of elongated cells were clearly seen in control embryos (A,B), only two dorsal protruding papillae were present in treated larvae (G,H) [B,H: phalloidin (white) and DAPI (cyan) in confocal sections; A,G: resulting surface rendering]. (C,I) Double fluorescence *in situ* hybridization for *Pou4* (magenta) and *Isl* (green) in control (C) and treated (I) embryos at late tailbud stages (St. 23). Whereas three spots of *Isl* expression were seen in control embryos (*n*=3), two dorsal spots were detected in all treated embryos (*n*=4). In the ventral region, *Pou4* was expressed in two cells in controls (as described in Fig. 5). In treated embryos, we found two embryos with two *Pou4*+ cells and two embryos with one *Pou4*+ cell. White arrows in I point to two *Pou4*+ cells in the ventral area of a treated embryo. (D,J) Fluorescence *in situ* hybridization for *Msx* (magenta) in control (D) and treated (J) embryos at early tailbud stages (St. 19). Control embryos: 100% with *Msx* expression in the ventral palp region (*n*=4). BMP2-treated embryos: 100% without *Msx* expression (*n*=12). (E,F,K,L) Colorimetric *in situ* hybridization for *Sp6/7/8/9* (E,K) and *Sox14/15/21* (F,L). In these panels, n indicates the number of embryos examined. The percentages indicate the frequency of the phenotype depicted in the image. Results were obtained from two independent experiments. White stars in I-K highlight the absence of staining in the ventral region. Embryos are shown with dorsal to the top in frontal views except lateral views in B and H. Scale bars: 25 μm (displayed for each type of imaging data).

final phenotypes (Fig. 7U-X). Importantly, our data show that the dorsal-most cells of the *Foxg* U-shape and dorsal palps develop independently of BMP signaling. In conclusion, we propose that the ventral papilla and the papilla versus inter-papilla fate choice is controlled by BMP signaling through the indirect regulation of *Sp6/7/8/9* expression.

Palp formation is similarly regulated by BMP in *P. mammillata*

We investigated the conservation of the role of BMP in palp formation by examining embryos of the ascidian *P. mammillata*, which belongs to the same family as *Ciona*, the Phlebobranchia, but with a significant divergence time (275 My) (Fig. 8A) (Delsuc et al., 2018). First, we determined that BMP signaling was active in the ventral part of the embryo with a similar dynamic to *Ciona* as revealed by P-Smad1/5/8 immunostaining (Fig. S4). Next, we identified single orthologs for *Celf3/4/5/6*, *Pou4* and *Isl* genes, which were all expressed in the palps (Fig. 8B,E,I,M) (Chowdhury et al., 2022; Coulcher et al., 2020; Dardaillon et al., 2020). Treatment with recombinant BMP2 protein from the 8-cell stage abolished expression of all three markers in the palps, like in *Ciona* (Fig. 8C,F,J,N). Following DMH1 treatment from the 8-cell stage, both *Celf3/4/5/6* and *Isl* were expressed in the palp territory following a U-shape pattern like in *Ciona*, but not in all cases. For a large fraction of embryos, the pattern appeared as two bars of intense staining resembling the U-shape but without the ventral part (Fig. 8D,G,H,K,L). This phenotype, which we did not observe in *Ciona*, might reveal some differences in the role of BMP in the two species.

Given the overall similar effects on palp formation after alterations of BMP signaling, we sought to identify novel palp molecular markers using a dataset previously generated in *P. mammillata* (Chowdhury et al., 2022). In this previous study, we generated, at several developmental stages, RNA-seq data for whole embryos treated with recombinant BMP4 protein and/or DAPT, a pharmacological Notch inhibitor. We identified 1098 genes

repressed by BMP signaling at least at one developmental stage (Table S1). In this list, we found the orthologs for 11 well-defined *Ciona* palp markers, and four of them (*Otx*, *Isl*, *Atoh1/7* and *Celf3/4/5/6*) have been described as expressed in the palp lineage in *Phallusia* (Coulcher et al., 2020; Dardaillon et al., 2020). Using Gene Ontology analysis, we selected a list of 53 genes encoding developmental regulators (transcription factors and signaling molecules) or involved in neural tissue formation, and examined their expression patterns (Table S2). Within this list, the expression patterns of 26 genes were previously determined [from the Aniseed database (Dardaillon et al., 2020) and from our previous data (Chowdhury et al., 2022; Coulcher et al., 2020)] and 12 of them were expressed in the palps. We performed *in situ* hybridization for the remaining 27 genes, and discovered eight novel palp markers (*Tp53inp*, *Fzd9/10*, *Plg*, *Mucin*, *Hes.b*, *Barhl*, *Fbn* and *Wscd*), expression of which is shown in Fig. 9.

Surprisingly, by examining the expression data generated previously, we found that some genes with palp expression were upregulated by BMP in our dataset, such as *Chrdl* and *Nos* (Table S2, Fig. 9A,K). To have a broader view of the potential effects of BMP signaling on gene regulation in the palps, we gathered, from previous publications (Chen et al., 2011; Chowdhury et al., 2022; Coulcher et al., 2020; Joyce Tang et al., 2013; Kusakabe et al., 2012; Liu and Satou, 2019; Pasini et al., 2006; Roure and Darras, 2016; Shimeld et al., 2005; Wagner and Levine, 2012; Wagner et al., 2014), from the Aniseed database (Dardaillon et al., 2020) and from the present study, a list of 68 genes with expression in the palp lineage in *Ciona* and/or *Phallusia* (Table S3). We plotted the results of our *Phallusia* RNA-seq data, and found that 70% of the genes were regulated by BMP signaling. Most of them were repressed by BMP, but 20 genes were activated by BMP, and a smaller fraction was repressed or activated depending on the stage. Consequently, the precise function of BMP, which is likely to be dynamic in the course of palp differentiation, needs to be investigated in further detail. Interestingly, Notch is likely to play a role in the specification of the different cell types that
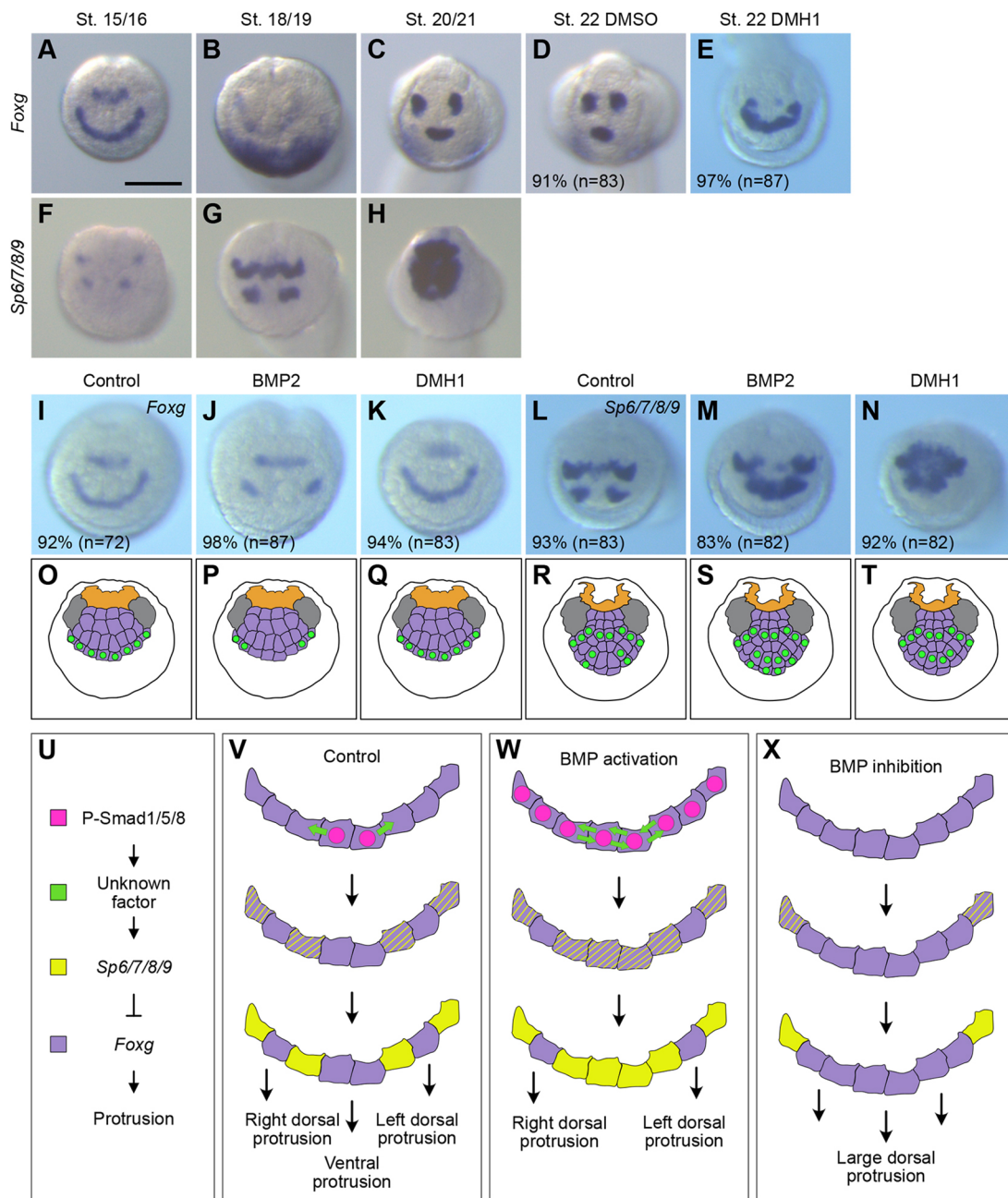
Fig. 7. Regulation of *Foxg* and *Sp6/7/8/9* by BMP signaling. (A-D) Expression of *Foxg* at different developmental stages in the palp-forming area. The specific stage is indicated at the top of each image. Note that, at early stages (A), *Foxg* was expressed in two anterior ectodermal territories, the U-shaped palp-forming region and a more dorsal row of cells likely contributing to the oral siphon primordium (Liu and Satou, 2019). At initial tailbud stages (B) *Foxg* expression was dramatically downregulated in the U-shaped region. Concomitantly, a transient strong expression in the ventral trunk epidermis was detected. (E) At mid tailbud stages, *Foxg* was expressed following a U-shape when the BMP pathway was inhibited from early gastrula (St. 10) with DMH1 when compared with control embryo (D). (F-H) *Sp6/7/8/9* expression at different developmental stages in the palp-forming area. (I-N) Expression of *Foxg* (I-K) at late neurula stages (St. 16) and *Sp6/7/8/9* (L-N) at initial tailbud stages (St. 18) in control embryos (I,L), BMP2-treated embryos (J,M) and DMH1-treated embryos (K,N). n indicates the number of embryos examined. The percentages indicate the frequency of the phenotype depicted in the picture. Results obtained from two independent experiments. Embryos are shown in frontal view with dorsal to the top. Scale bar: 50 µm. (O-T) Schematics of our interpretation of the expression patterns is shown for *Foxg* (O-Q) and *Sp6/7/8/9* (R-T) with the same color code as in Fig. 2 (purple: palp precursors; orange: a-line CNS; gray: aATEN precursors; green: gene expression). (U-X) Model for the action of BMP signaling on protruding papilla versus inter-palp fate specification. The model focuses on the eight *Foxg*^{+} cells making a U-shape at neurula stages, which have the potential to become protruding papillae. Importantly, dorsal palp formation is independent of BMP signaling, and expression data (I-N) show that only the four median cells are affected by BMP signaling. Hence, the model focuses only on these four cells where we postulate some genetic interactions (U). During normal development (V), active BMP signaling (magenta) in the two median cells induces ventral fate and the expression of an unidentified factor (green), which activates the expression of *Sp6/7/8/9* (yellow) in the neighboring cells (*Sp6/7/8/9* is also activated independently of BMP in the most dorsal cells). Next, Sp6/7/8/9 represses the expression of *Foxg* (purple) leading to alternate and excluded patterns of expression of these two genes and subsequent specification of protruding and non-protruding cells. Following BMP activation (W), the unidentified factor activates *Sp6/7/8/9* in the four median cells, abolishing *Foxg* expression and the formation of the ventral protrusion. In the absence of BMP signaling (X), median cells do not acquire a ventral identity and do not express the unidentified factor. Hence, *Sp6/7/8/9* expression is not activated and *Foxg* not repressed.
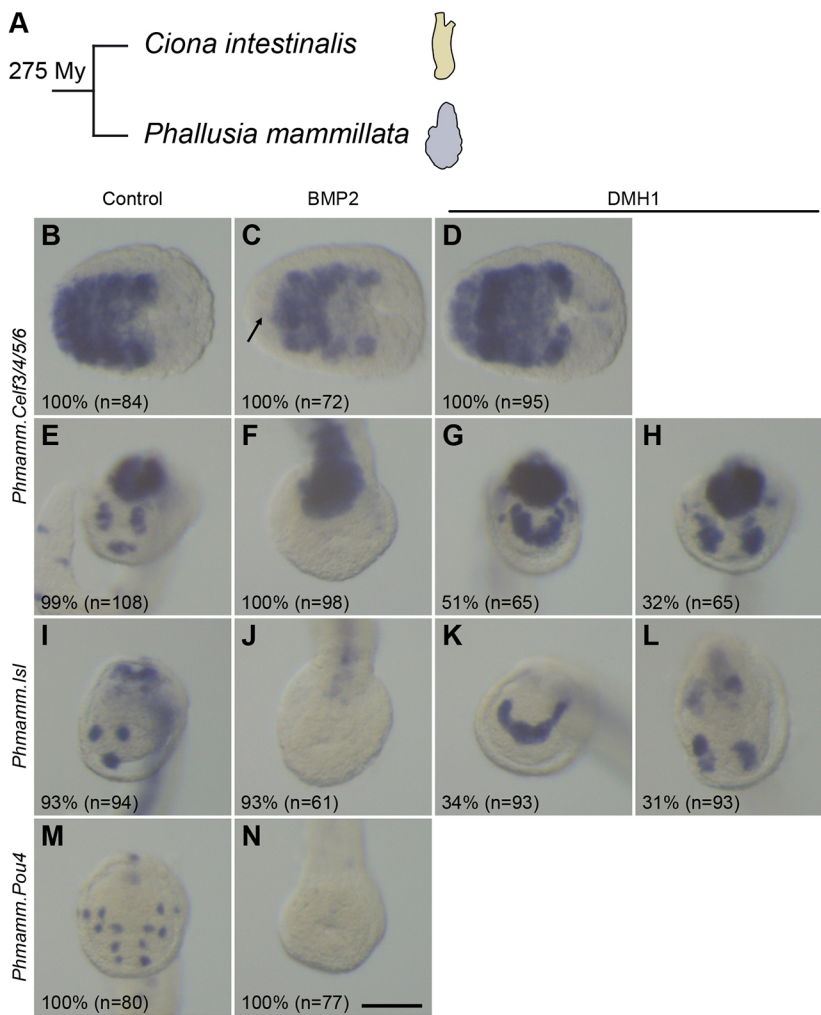
Fig. 8. The BMP signaling pathway regulates palp formation in *P. mammillata*. (A) Schematics of the appearance of adult *C. intestinalis* and *P. mammillata*, and their phylogenetic distance. (B-N) *P. mammillata* embryos were treated from the 8-cell stage with 150 ng/ml recombinant BMP2 protein (C,F,J,N) or 2.5 μM DMH1 (D,G,H,K,L). They were fixed at neurula stages (B-D) and mid/late tailbud (E-N) stages. Expression patterns for *Celf3/4/5/6* (B-H), *Isl* (I-L) and *Pou4* (M,N) were determined by *in situ* hybridization. The arrow in C marks the repression of *Celf3/4/5/6* in the ANB. For each panel, n indicates the number of embryos examined. The percentages indicate the frequency of the phenotype depicted in the picture. Results obtained from two or more independent experiments. Embryos are shown with anterior to the left in neural plate view (B-D), and in frontal view with dorsal to the top (E-N). Scale bar: 50 μm.

compose the palps. For instance, it has been shown that activating Notch represses palp neuronal markers in *H. roretzi* (Akanuma et al., 2002). We found 30 genes regulated by Notch in our dataset.

DISCUSSION

We have shown that BMP signaling regulates two distinct steps of palp formation in *C. intestinalis*: ANB specification, and ventral papilla versus inter-papilla specification. Moreover, we have shown conservation of gene expression and regulation by BMP in *P. mammillata*.

Signaling pathway inhibition and ANB specification

ANB specification is regulated by inputs from several signaling pathways: FGF, Wnt and BMP. Although FGF is positively required early on, at the time of neural induction (32-cell stage), all three pathways are inactive at the time of ANB fate acquisition as revealed by the expression of *Foxc* (mid-gastrula). This situation is reminiscent of data from vertebrates wherein anterior neural fate is determined by the triple inhibition of BMP, Nodal and Wnt pathways (Andoniadou and Martinez-Barbera, 2013; Niehrs et al., 2003; Wilson and Houart, 2004). It would thus be interesting to test the function of Nodal inhibition in ANB specification given that we have already shown that it is involved in posterior neural fate determination in *Ciona* (Roure et al., 2014). Although it appears that active FGF, Wnt or BMP signaling is incompatible with ANB determination, the specific function of each pathway seems different. FGF appears to regulate the anterior CNS versus ANB fate decision along the antero-posterior axis (Wagner and Levine, 2012). Wnt seems to regulate *Foxc*+ ANB fate versus *Foxc*− ANB fate along the mediolateral/dorsoventral axis (Feinberg et al., 2019). Finally, BMP might participate in the segregation between ANB and immediately anterior/ventral epidermal fates. Finer details on the function of these pathways in ANB fate determination and on their likely cross-talk should be an exciting line of research in this simple and geometric model system.

From ANB to palp differentiation

Our results of late inhibition of BMP signaling (from gastrula stages) indicate that *Foxg*, expressed in a single row of cells with a U-shape, delineates cells competent to become papilla. A network of gene interactions has previously been identified that regulates the transition of *Foxg* from a U-shape to a three-spot pattern eventually forming protruding papillae (Liu and Satou, 2019). BMP is an input to this network, presumably through the indirect regulation of ventral *Sp6/7/8/9* expression. We hypothesized the involvement of a signaling molecule that would be a direct target of BMP (Fig. 7). Interestingly, MAPK inhibition during neurulation results in a U-shaped expression of *Isl* (Wagner et al., 2014), similar to what we observed by inhibiting BMP. It is tempting to propose an FGF ligand to be the factor downstream of BMP; however, none has been described with a discrete pattern in the palps (Imai et al., 2004). Again, studying epistatic relationships and cross-talk between these signaling pathways is a future line of research.
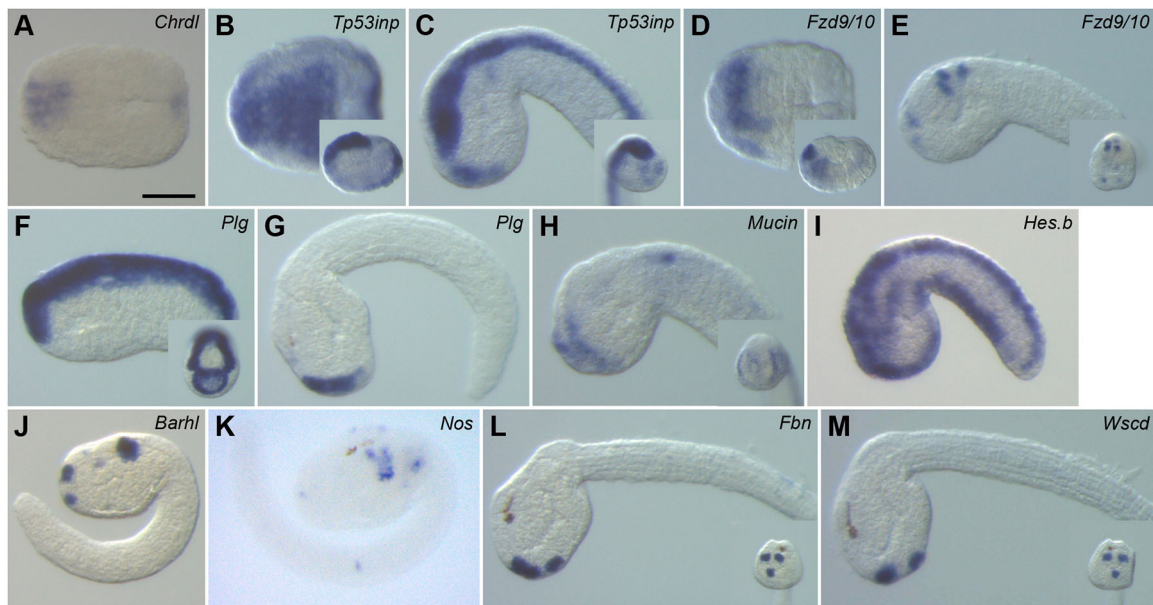
Fig. 9. Identification of genes expressed in the palps in *P. mammillata*. (A-M) *In situ* hybridization at selected stages for *Chrdl* (A), *Tp53inp* (B,C), *Fzd9/10* (D,E), *Plg* (F,G), *Mucin* (H), *Hes.b* (I), *Barhl* (J), *Nos* (K), *Fbn* (L) and *Wscd* (M). Embryos are shown with anterior to the left in neural plate view (A,B,D), in lateral view with dorsal to the top (B inset,C,D inset, E-M), and in frontal view with dorsal to the top (insets in C,E,F,H,L,M). Scale bar: 50 µm.

Importantly, we have shown that BMP signaling is active and required in the median palp-forming region, most likely corresponding to the future ventral palp, before the onset of *Foxg* and *Sp6/7/8/9* expression. However, activating BMP at this stage does not result in ectopic palp formation but rather to an absence of the ventral palp. This discrepancy might be better understood by more fine control of the levels of BMP signaling, but also its timing and the cells that receive it, through optogenetics for example. Nevertheless, our observations point to differences between the two symmetrically bilateral dorsal palps and the single median ventral palp. Although we are not aware of ventral palp-specific marker, we have shown that *Msx* is transiently expressed only in the ventral palp (Fig. 5); this may also be the case for *Hes.a* (Chowdhury et al., 2022). In addition, the $Pou4^+$ sensory neurons are located dorsally in the ventral palp, whereas they are located around Isl^+ cells in the dorsal palps. Specific dorsal and ventral genetic sub-networks would thus be interesting to uncover.

Anterior adhesive organ formation in chordates

The specification of the three cell types (ACCs, neurons and collocytes) that make the papillae and their relationships (e.g. lineage, alternative cell fate) are still poorly understood, but will most likely be the subject of future research (Zeng et al., 2019). For example, we are not aware of a collocyte-specific gene marker; however, these cells can be distinguished from other palp cells with peanut agglutinin (Cao et al., 2019; Sato and Morisawa, 1999; Zeng et al., 2019). The collocytes are involved in the secretion of adhesive materials for the larva to attach to a substrate before metamorphosis. The palps thus constitute an adhesive organ homology of which with adhesive organs that exist in the larvae of some vertebrates (e.g. the cement gland of *Xenopus*) has been previously proposed (Yoshida et al., 2012). Our present work adds to the similarities observed between the frog cement gland and ascidian palps: they are ectodermal derivatives specialized in adhesion, they are located at the anterior-most part of the larva, they share expression of the transcription factor-coding genes *Otx* and *Pitx*, and their formation is regulated by BMP

signaling (Gammill and Sive, 2000; Jin and Weinstein, 2018; Yoshida et al., 2012). Further detailed comparison of the shared, but also divergent, parts of the developmental networks regulating adhesive organ/sensory organ formation in ascidians and vertebrates should be of great interest.

Possible conservation of PNS formation in chordates

The ascidian larval PNS, palps included, originates from the neural plate border with the exception of the ventral tail PNS, which originates from a region at the opposite end of the embryo, the ventral epidermis. Signaling pathways are pleiotropic and are consequently poor indicators of possible evolutionary conservation. Nevertheless, it is striking that FGF, Wnt and BMP are deployed in ascidians to regulate neural plate border specification and differentiation of its derivatives, most likely with changing dynamic requirements at diverse developmental stages. This is reminiscent of the mechanisms regulating the neural plate border and its derivatives, the cranial placodes and the neural crest (Martik and Bronner, 2021; Pla and Monsoro-Burq, 2018; Stundl et al., 2021). The similarities extend beyond signaling pathways as a suite of genes have conserved expression between ascidians and vertebrates, and have led to the proposal of several evolutionary scenarios (Cao et al., 2019; Horie et al., 2018; Pasini et al., 2006; Poncelet and Shimeld, 2020). Our present study adds further useful information to gene network level comparisons.

The ascidian PNS comprises epidermal sensory neurons that have different morphologies, connectivity and sensory capacities depending on their location (Abitua et al., 2015; Imai and Meinertzhagen, 2007; Ryan et al., 2018). However, they share a number of genes marking the presumptive domains or differentiating neurons. Yet, what regulates their specific identities is still incompletely understood (Chacha et al., 2022). For example, a number of genes expressed in the tail PNS are also expressed in the palps, and these expression domains are conserved in species that diverged almost 400 My ago (Table S3) (Akanuma et al., 2002; Coulcher et al., 2020; Joyce Tang et al., 2013; Pasini et al., 2006;

Roure and Darras, 2016). Comparative approaches of PNS formation between divergent ascidian species and across chordates (vertebrates and cephalochordates) promise to yield insights into PNS evolution and the flexibility of developmental mechanisms.

MATERIALS AND METHODS

Embryo obtention and manipulation

Adults from *Ciona intestinalis* (formerly referred to *Ciona intestinalis* type B; Brunetti et al., 2015) were provided by the Centre de Ressources Biologiques Marines in Roscoff (EMBRC-France). Adults of *Phallusia mammillata* were provided by the Centre de Ressources Biologiques Marines in Banyuls-sur-Mer (EMBRC-France) following diving or by professional fishermen following trawling in the Banyuls-sur-Mer (France) area. Gamete collection, *in vitro* fertilization, dechorionation and electroporation were performed as previously described (Coulcher et al., 2020; Darras, 2021), and staging of embryos was performed according to the developmental table of *Ciona robusta* (Hotta et al., 2007).

Electroporation constructs used in this study have been previously described (Pasini et al., 2006). Embryos were treated with 150 ng/ml of recombinant mouse BMP2 protein [355-BEC, R&D Systems; 100 µg/ml stock solution in 4 mM HCl+0.1% bovine serum albumin (BSA)], 100 ng/ml of recombinant human bFGF (F0291, Sigma-Aldrich; 50 µg/ml stock solution in 20 mM Tris pH 7.5+0.1% BSA) complemented with 0.1% BSA, or 2.5 µM of the BMP receptor inhibitor DMH1 (S7146, Euromedex; 10 mM stock solution in DMSO) at the stages indicated in the text and figures. These concentrations were determined following pilot experiments. Control embryos were incubated with sea water containing 0.1% BSA and/or 0.025% DMSO.

In situ hybridization and immunostaining

For all labeling experiments, embryos were fixed in 0.5 M NaCl, 100 mM MOPS pH 7.5 and 3.7% formaldehyde. Whole-mount chromogenic *in situ* hybridization was performed using plasmid cDNA or synthetic DNA (eBlocks Gene Fragment, IDT) as templates for probe synthesis (Tables S2 and S4) as described previously (Chowdhury et al., 2022). Gene models and identifiers correspond to the genome assemblies KH2012 for *Ciona robusta* (Satou et al., 2008) and MTP2014 for *Phallusia mammillata*, which were retrieved from the Aniseed database (Dardaillon et al., 2020). Images were acquired using an AxioCam ERc5 s digital camera mounted on a stereomicroscope (Discovery V20, Zeiss). The numbers of experiments and embryos for phenotypic effects by gene expression analysis are shown in the figures and their legends.

The fluorescence *in situ* hybridization protocol was adapted from that described by Racioppi et al. (2014). Briefly, digoxigenin-labeled probes were recognized using an anti-DIG antibody coupled to peroxidase (11207733910, Roche), and fluorescein-labeled probes were recognized using an anti-FLUO antibody coupled to peroxidase (11426346910, Roche). Fluorescence signal was produced using the TSA plus kit (NEL753001KT, PerkinElmer) following the manufacturer's recommendations with Cy3 and fluorescein for DIG- and FLUO-probes, respectively. Active BMP signaling was visualized by immunostaining using a rabbit monoclonal antibody against mammal Smad1, Smad5 and Smad8 phosphorylated at two serine residues at the C-terminal end (clone 41D10, #9516, Cell Signaling Technology) diluted at 1:200. The epitope is present in the single ortholog Smad1/5/8 of both *Ciona intestinalis* and *Phallusia mammillata*. Anti-rabbit antibodies coupled to Alexa Fluor 568 (A11011, Invitrogen) were used at 1:400 for visualization. Similar data were obtained using another antibody (clone D5B10, #13820, Cell Signaling Technology) (data not shown). Membranes were stained using Alexa Fluor 594 phalloidin (A12381, Invitrogen) used at 1:1000. Nuclei were stained using DAPI. Image acquisition was performed using confocal microscopy (Leica SP8-X, BioPiC platform, Banyuls-sur-Mer). Confocal *z*-stacks were visualized and analyzed in 3D using the Imaris 8.3 software (Bitplane). In particular, this software was used to count the number of cells expressing a gene of interest. In brief, fluorescence signals were converted as 3D objects:

in situ hybridization signals as surface objects, and DAPI-labeled nuclei as spots. The number of spots within a given surface was used as a proxy for the number of cells expressing a gene. Snapshots of such analyses and 3D renderings are shown in Figs 1, 2, 5, 6 and Figs S1, S2. Maximum intensity projections of Fig. S4 were obtained using ImageJ.

Image panels and figures were constructed with Affinity Photo and Affinity Designer.

References

Abitua, P. B., Gainous, T. B., Kaczmarczyk, A. N., Winchell, C. J., Hudson, C., Kamata, K., Nakagawa, M., Tsuda, M., Kusakabe, T. G. and Levine, M. (2015). The pre-vertebrate origins of neurogenic placodes. *Nature* **524**, 462-465. doi:10.1038/nature14657

Akanuma, T., Hori, S., Darras, S. and Nishida, H. (2002). Notch signaling is involved in nervous system formation in ascidian embryos. *Dev. Genes Evol.* **212**, 459-472. doi:10.1007/s00427-002-0264-x

**Andoniadou, C. L. and Martinez-Barbera, J. P.** (2013). Developmental mechanisms directing early anterior forebrain specification in vertebrates. *Cell. Mol. Life Sci.* **70**, 3739-3752. doi:10.1007/s00018-013-1269-5

Brunetti, R., Gissi, C., Pennati, R., Caicci, F., Gasparini, F. and Manni, L. (2015). Morphological evidence that the molecularly determined *Ciona intestinalis* type A and type B are different species: *Ciona robusta* and *Ciona intestinalis*. *J. Zool. Syst. Evol. Res.* **53**, 186-193. doi:10.1111/jzs.12101

Cao, C., Lemaire, L. A., Wang, W., Yoon, P. H., Choi, Y. A., Parsons, L. R., Matese, J. C., Wang, W., Levine, M. and Chen, K. (2019). Comprehensive single-cell transcriptome lineages of a proto-vertebrate. *Nature* **571**, 349-354. doi:10.1038/s41586-019-1385-y

Chacha, P. P., Horie, R., Kusakabe, T. G., Sasakura, Y., Singh, M., Horie, T. and Levine, M. (2022). Neuronal identities derived by misexpression of the POU IV sensory determinant in a protovertebrate. *Proc. Natl. Acad. Sci. USA* **119**, e2118817119. doi:10.1073/pnas.2118817119

Chen, J. S., Pedro, M. S. and Zeller, R. W. (2011). miR-124 function during Ciona intestinalis neuronal development includes extensive interaction with the Notch signaling pathway. *Development* **138**, 4943-4953. doi:10.1242/dev.068049

Chowdhury, R., Roure, A., le Pétillon, Y., Mayeur, H., Daric, V. and Darras, S. (2022). Highly distinct genetic programs for peripheral nervous system formation in chordates. *BMC Biol.* **20**, 1-25. doi:10.1186/s12915-022-01355-7

Cloney, R. A. (1977). Larval adhesive organs and metamorphosis in ascidians - I. Fine structure of the everting papillae of Distaplia occidentalis. *Cell Tissue Res.* **183**, 423-444. doi:10.1007/BF00225658

Coulcher, J. F., Roure, A., Chowdhury, R., Robert, M., Lescat, L., Bouin, A., Carvajal Cadavid, J., Nishida, H. and Darras, S. (2020). Conservation of
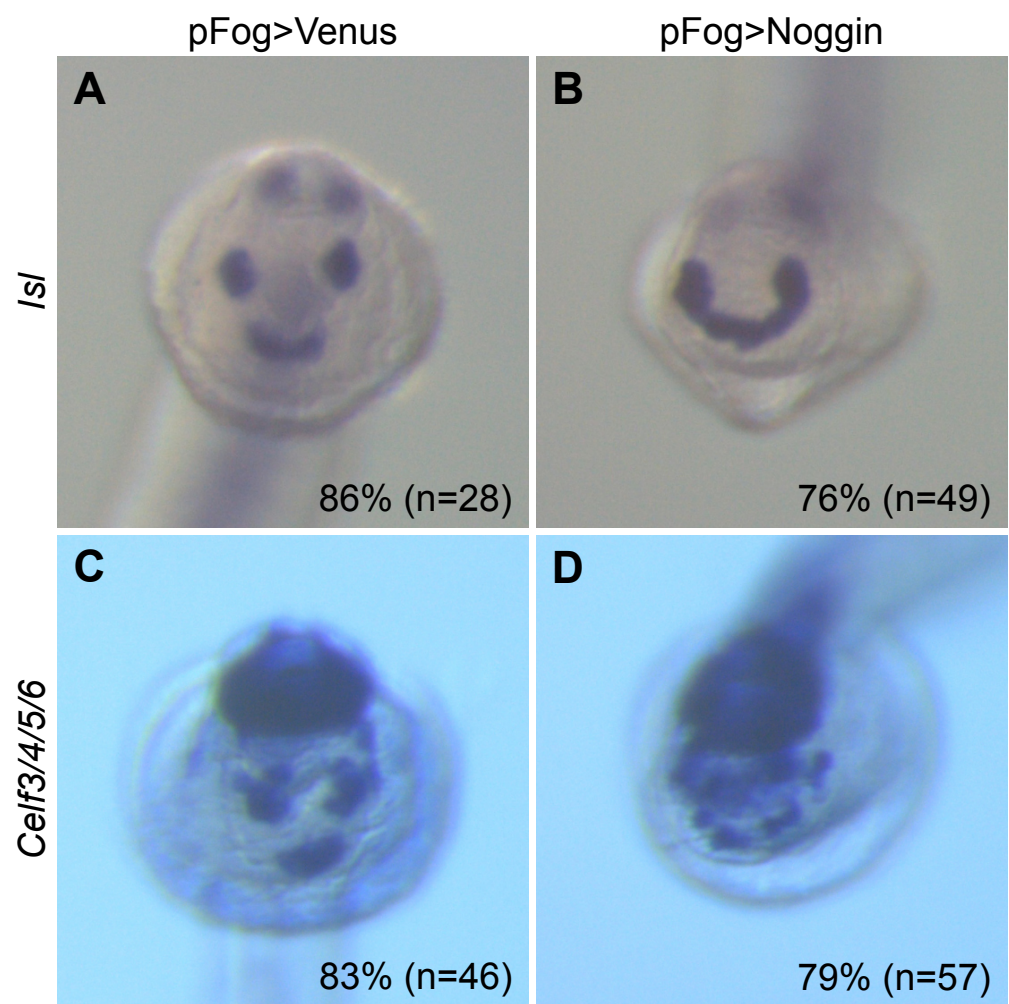
peripheral nervous system formation mechanisms in divergent ascidian embryos. *eLife* **9**, e59157. doi:10.7554/eLife.59157

Dardaillon, J., Dauga, D., Simion, P., Faure, E., Onuma, T. A., DeBiasse, M. B., Louis, A., Nitta, K. R., Naville, M., Besnardeau, L. et al. (2020). ANISEED 2019: 4D exploration of genetic data for an extended range of tunicates. *Nucleic Acids Res.* **48**, D668-D675.

Darras, S. (2021). En masse DNA electroporation for in vivo transcriptional assay in ascidian embryos. *Bio-protocol* **11**, e4160. doi:10.21769/BioProtoc.4160

Darras, S. and Nishida, H. (2001). The BMP/CHORDIN antagonism controls sensory pigment cell specification and differentiation in the ascidian embryo. *Dev. Biol.* **236**, 271-288. doi:10.1006/dbio.2001.0339

Delsuc, F., Brinkmann, H., Chourrout, D. and Philippe, H. (2006). Tunicates and not cephalochordates are the closest living relatives of vertebrates. *Nature* **439**, 965-968. doi:10.1038/nature04336

Delsuc, F., Philippe, H., Tsagkogeorga, G., Simion, P., Tilak, M.-K., Turon, X., López-Legentil, S., Piette, J., Lemaire, P. and Douzery, E. J. P. (2018). A phylogenomic framework and timescale for comparative studies of tunicates. *BMC Biol.* **16**, 39. doi:10.1186/s12915-018-0499-2

Feinberg, S., Roure, A., Piron, J. and Darras, S. (2019). Antero-posterior ectoderm patterning by canonical Wnt signaling during ascidian development. *PLoS Genet.* **15**, e1008054. doi:10.1371/journal.pgen.1008054

Gammill, L. S. and Sive, H. (2000). Coincidence of otx2 and BMP4 signaling correlates with Xenopus cement gland formation. *Mech. Dev.* **92**, 217-226. doi:10.1016/S0925-4773(99)00342-1

Guignard, L., Fiúza, U.-M., Leggio, B., Laussu, J., Faure, E., Michelin, G., Biasuz, K., Hufnagel, L., Malandain, G., Godin, C. et al. (2020). Contact area-dependent cell communication and the morphological invariance of ascidian embryogenesis. *Science* **369**, eaar5663. doi:10.1126/science.aar5663

Horie, R., Hazbun, A., Chen, K., Cao, C., Levine, M. and Horie, T. (2018). Shared evolutionary origin of vertebrate neural crest and cranial placodes. *Nature* **560**, 228-232. doi:10.1038/s41586-018-0385-7

Hotta, K., Mitsuhara, K., Takahashi, H., Inaba, K., Oka, K., Gojobori, T. and Ikeo, K. (2007). A web-based interactive developmental table for the ascidian Ciona intestinalis, including 3D real-image embryo reconstructions: I. From fertilized egg to hatching larva. *Dev. Dyn.* **236**, 1790-1805. doi:10.1002/dvdy.21188

Hudson, C. (2016). The central nervous system of ascidian larvae: Nervous system development in ascidians. *Wiley Interdiscip. Rev. Dev. Biol.* **5**, 538-561. doi:10.1002/wdev.239

Hudson, C., Darras, S., Caillol, D., Yasuo, H. and Lemaire, P. (2003). A conserved role for the MEK signalling pathway in neural tissue specification and posteriorisation in the invertebrate chordate, the ascidian Ciona intestinalis. *Development* **130**, 147-159. doi:10.1242/dev.00200

Imai, J. H. and Meinertzhagen, I. A. (2007). Neurons of the ascidian larval nervous system in Ciona intestinalis: II. Peripheral nervous system. *J. Comp. Neurol.* **501**, 335-352. doi:10.1002/cne.21247

Imai, K. S., Hino, K., Yagi, K., Satoh, N. and Satou, Y. (2004). Gene expression profiles of transcription factors and signaling molecules in the ascidian embryo: towards a comprehensive understanding of gene networks. *Development* **131**, 4047-4058. doi:10.1242/dev.01270

Imai, K. S., Levine, M., Satoh, N. and Satou, Y. (2006). Regulatory blueprint for a chordate embryo. *Science* **312**, 1183-1187. doi:10.1126/science.1123404

Jin, Y. and Weinstein, D. C. (2018). Pitx1 regulates cement gland development in Xenopus laevis through activation of transcriptional targets and inhibition of BMP signaling. *Dev. Biol.* **437**, 41-49. doi:10.1016/j.ydbio.2018.03.008

Johnson, C. J., Razy-Krajka, F. and Stolfi, A. (2020). Expression of smooth muscle-like effectors and core cardiomyocyte regulators in the contractile papillae of Ciona. *EvoDevo* **11**, 15. doi:10.1186/s13227-020-00162-x

Joyce Tang, W., Chen, J. S. and Zeller, R. W. (2013). Transcriptional regulation of the peripheral nervous system in Ciona intestinalis. *Dev. Biol.* **378**, 183-193. doi:10.1016/j.ydbio.2013.03.016

Kusakabe, T. G., Sakai, T., Aoyama, M., Kitajima, Y., Miyamoto, Y., Takigawa, T., Daido, Y., Fujiwara, K., Terashima, Y., Sugiuchi, Y. et al. (2012). A conserved non-reproductive GnRH system in chordates. *PLoS ONE* **7**, e41955. doi:10.1371/journal.pone.0041955

Leggio, B., Laussu, J., Carlier, A., Godin, C., Lemaire, P. and Faure, E. (2019). MorphoNet: an interactive online morphological browser to explore complex multi-scale data. *Nat. Commun.* **10**, 2812. doi:10.1038/s41467-019-10668-1

Liu, B. and Satou, Y. (2019). Foxg specifies sensory neurons in the anterior neural plate border of the ascidian embryo. *Nat. Commun.* **10**, 4911. doi:10.1038/s41467-019-12839-6

Martik, M. L. and Bronner, M. E. (2021). Riding the crest to get a head: neural crest evolution in vertebrates. *Nat. Rev. Neurosci.* **22**, 616-626. doi:10.1038/s41583-021-00503-2

Niehrs, C., Kazanskaya, O., Wu, W. and Glinka, A. (2003). Dickkopf1 and the Spemann-Mangold head organizer. *Int. J. Dev. Biol.* **45**, 237-240.

Nishida, H. (1987). Cell lineage analysis in ascidian embryos by intracellular injection of a tracer enzyme. III. Up to the tissue restricted stage. *Dev. Biol.* **121**, 526-541. doi:10.1016/0012-1606(87)90188-6

Pasini, A., Amiel, A., Rothbacher, U., Roure, A., Lemaire, P. and Darras, S. (2006). Formation of the ascidian epidermal sensory neurons: insights into the origin of the chordate peripheral nervous system. *PLoS Biol.* **4**, e225. doi:10.1371/journal.pbio.0040225

Pennati, R. and Rothbächer, U. (2015). Bioadhesion in ascidians: a developmental and functional genomics perspective. *Interface Focus* **5**, 20140061. doi:10.1098/rsfs.2014.0061

Pla, P. and Monsoro-Burq, A. H. (2018). The neural border: Induction, specification and maturation of the territory that generates neural crest cells. *Dev. Biol.* **444**, S36-S46. doi:10.1016/j.ydbio.2018.05.018

Poncelet, G. and Shimeld, S. M. (2020). The evolutionary origins of the vertebrate olfactory system. *Open Biol.* **10**, 200330. doi:10.1098/rsob.200330

Racioppi, C., Kamal, A. K., Razy-Krajka, F., Gambardella, G., Zanetti, L., di Bernardo, D., Sanges, R., Christiaen, L. A. and Ristoratore, F. (2014). Fibroblast growth factor signalling controls nervous system patterning and pigment cell formation in Ciona intestinalis. *Nat. Commun.* **5**, 4830. doi:10.1038/ncomms5830

Rothbacher, U., Bertrand, V., Lamy, C. and Lemaire, P. (2007). A combinatorial code of maternal GATA, Ets and beta-catenin-TCF transcription factors specifies and patterns the early ascidian ectoderm. *Development* **134**, 4023-4032. doi:10.1242/dev.010850

Roure, A. and Darras, S. (2016). Msxb is a core component of the genetic circuitry specifying the dorsal and ventral neurogenic midlines in the ascidian embryo. *Dev. Biol.* **409**, 277-287. doi:10.1016/j.ydbio.2015.11.009

Roure, A., Lemaire, P. and Darras, S. (2014). An Otx/Nodal regulatory signature for posterior neural development in ascidians. *PLoS Genet.* **10**, e1004548. doi:10.1371/journal.pgen.1004548

Ryan, K., Lu, Z. and Meinertzhagen, I. A. (2018). The peripheral nervous system of the ascidian tadpole larva: Types of neurons and their synaptic networks. *J. Comp. Neurol.* **526**, 583-608. doi:10.1002/cne.24353

Sato, Y. and Morisawa, M. (1999). Loss of test cells leads to the formation of new tunic surface cells and abnormal metamorphosis in larvae of Ciona intestinalis (Chordata, ascidiacea). *Dev. Genes Evol.* **209**, 592-600. doi:10.1007/s004270050293

Satoh, N. (1994). *Developmental Biology of Ascidians*. Cambridge University Press.

Satou, Y., Mineta, K., Ogasawara, M., Sasakura, Y., Shoguchi, E., Ueno, K., Yamada, L., Matsumoto, J., Wasserscheid, J., Dewar, K. et al. (2008). Improved genome assembly and evidence-based global gene model set for the chordate Ciona intestinalis: new insight into intron and operon populations. *Genome Biol.* **9**, R152. doi:10.1186/gb-2008-9-10-r152

Shimeld, S. M., Purkiss, A. G., Dirks, R. P. H., Bateman, O. A., Slingsby, C. and Lubsen, N. H. (2005). Urochordate βγ-crystallin and the evolutionary origin of the vertebrate eye lens. *Curr. Biol.* **15**, 1684-1689. doi:10.1016/j.cub.2005.08.046

Stundl, J., Bertucci, P. Y., Lauri, A., Arendt, D. and Bronner, M. E. (2021). Evolution of new cell types at the lateral neural border. *Curr. Top. Dev. Biol.* **141**, 173-205. doi:10.1016/bs.ctdb.2020.11.005

Thawani, A. and Groves, A. K. (2020). Building the border: development of the chordate neural plate border region and its derivatives. *Front. Physiol.* **11**, 608880. doi:10.3389/fphys.2020.608880

Wagner, E. and Levine, M. (2012). FGF signaling establishes the anterior border of the Ciona neural tube. *Development* **139**, 2351-2359. doi:10.1242/dev.078485

Wagner, E., Stolfi, A., Gi Choi, Y. and Levine, M. (2014). Islet is a key determinant of ascidian palp morphogenesis. *Development* **141**, 3084-3092. doi:10.1242/dev.110684

Waki, K., Imai, K. S. and Satou, Y. (2015). Genetic pathways for differentiation of the peripheral nervous system in ascidians. *Nat. Commun.* **6**, 8719. doi:10.1038/ncomms9719

Wilson, S. W. and Houart, C. (2004). Early steps in the development of the forebrain. *Dev. Cell* **6**, 167-181. doi:10.1016/S1534-5807(04)00027-9

Yoshida, K., Ueno, M., Niwano, T. and Saiga, H. (2012). Transcription regulatory mechanism of Pitx in the papilla-forming region in the ascidian, Halocynthia roretzi, implies conserved involvement of Otx as the upstream gene in the adhesive organ development of chordates. *Dev. Growth Differ.* **54**, 649-659. doi:10.1111/j.1440-169X.2012.01366.x

Zeng, F., Wunderer, J., Salvenmoser, W., Hess, M. W., Ladurner, P. and Rothbächer, U. (2019). Papillae revisited and the nature of the adhesive secreting collocytes. *Dev. Biol.* **448**, 183-198. doi:10.1016/j.ydbio.2018.11.012
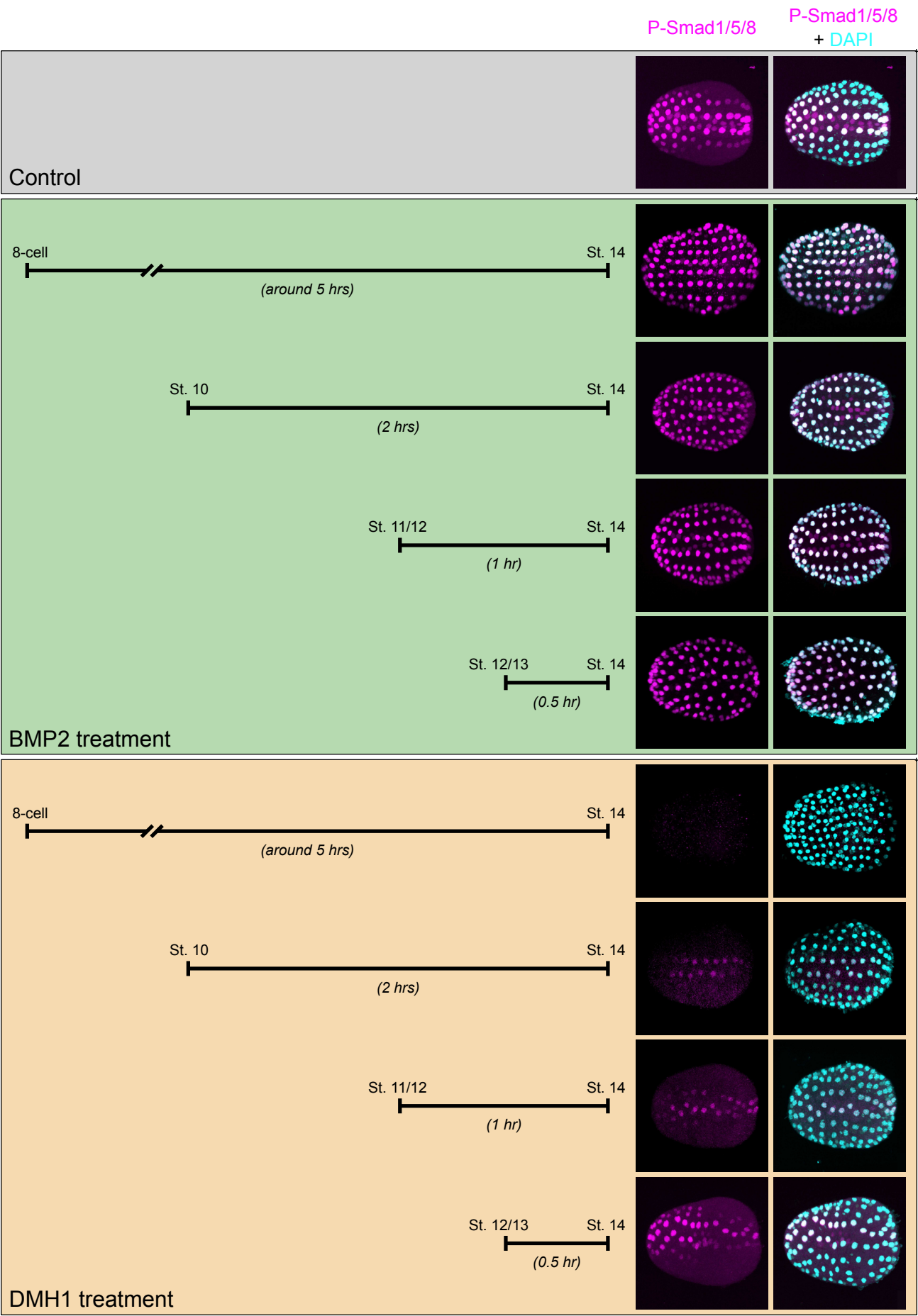
Fig. S1. Specificity of the P-Smad1/5/8 immunostaining. P-Smad1/5/8 immunostaining was performed on neurulae (St. 13/14). Active BMP signaling (magenta) was detected in nuclei of the ventral epidermis midline and the underlying endomesoderm in control embryos. Activation (treatment with BMP2 protein) and inhibition (treatment with DMH1) were started at progressively later stages indicated on the figure) and terminated at the time of fixation (St. 13/14). All treatments with BMP2, even the 30 min treatment, induced ectopic nuclear P-Smad1/5/8 throughout the epidermis. While DMH1 treatment from the 8-cell stage completely abolished P-Smad1/5/8 detection, shorter treatments strongly downregulated P-Smad1/5/8 levels. Embryos are shown in ventral views with anterior to the left (DAPI in cyan to highlight the nuclei). Scale bar: 20 µm. The experiment was performed once except the treatments from the 8-cell stage that have been analyzed in at least two independent experiments.

| | DAPI | *Foxc* | *Tfap2-r.b* | Merge |

Control
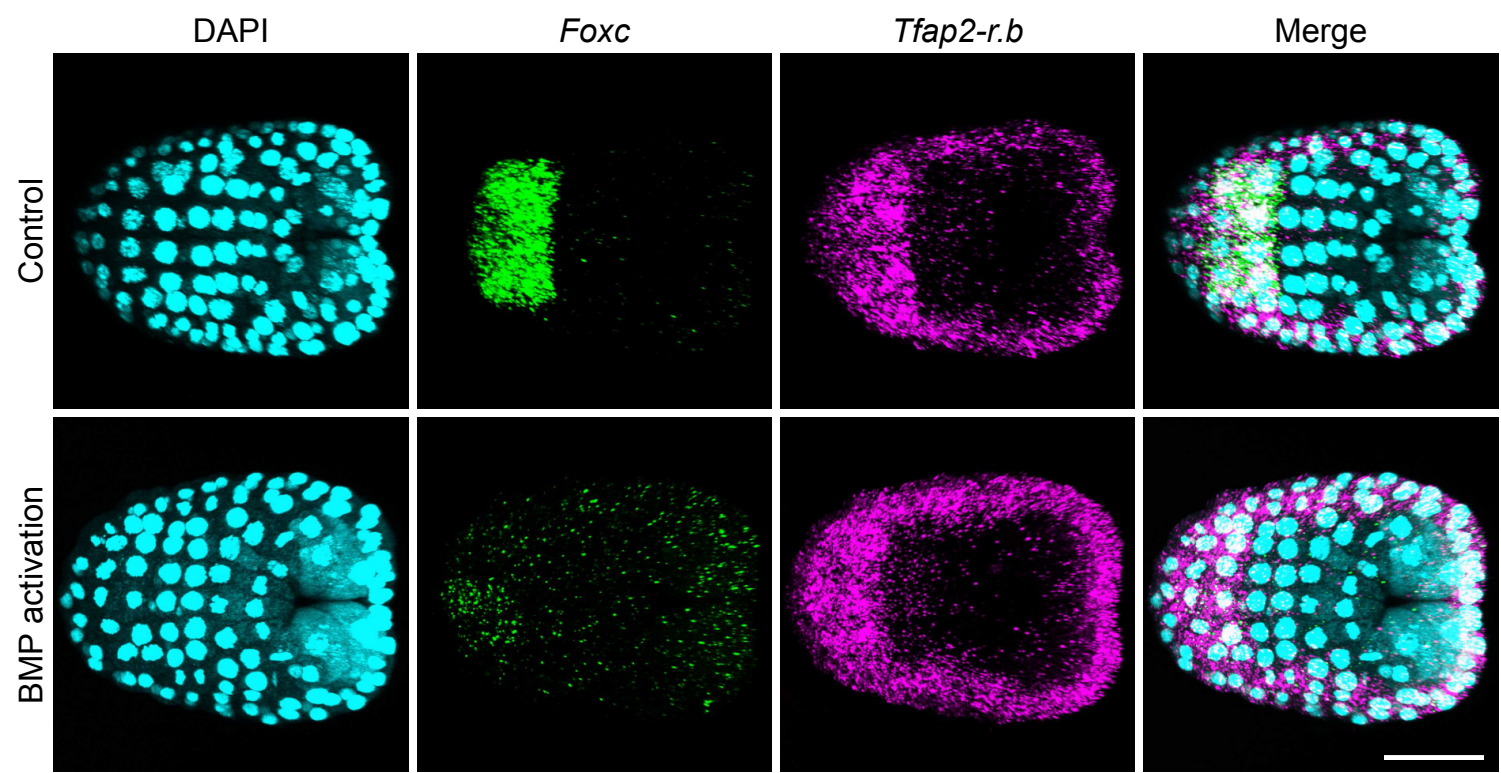
BMP activation

Fig. S2. Early BMP activation represses *Foxc* but not *Tfap2-r.b*. Embryos were treated with BMP2 protein and fixed at early neurula stages (St. 14) to determine *Foxc* (green) and *Tfap2-r.b* (magenta) expression by fluorescent *in situ* hybridization. In control embryos, *Foxc* was expressed in 8 cells that are also *Tfap2-r.b* positive (100%, n=6). By contrast, in treated embryos, *Foxc* was not detected while *Tfap2-r.b* expression was unchanged (100%, n=6). Embryos are shown in neural plate views with anterior to the left (DAPI in cyan to highlight the nuclei). Scale bar: 50 µm. The experiment was performed once.

pFog>Venus   pFog>Noggin

Isl

A 86% (n=28)   **B** 76% (n=49)

Celf3/4/5/6

C 83% (n=46)   **D** 79% (n=57)

Fig. S3. BMP inhibition by electroporation of pFog>Noggin alters palp formation. Embryos were electroporated with pFog>Venus (A,C) or pFog>Noggin (B,D) and fixed for *in situ* hybridization against *Isl* at mid tailbud stages (St.22) (A,B) and *Celf3/4/5/6* at late tailbud stages (St. 23) (C,D). For each panel, n indicates the number of embryos examined. The percentages indicate the frequency of the phenotype depicted in the picture. Each experiment has been performed once.
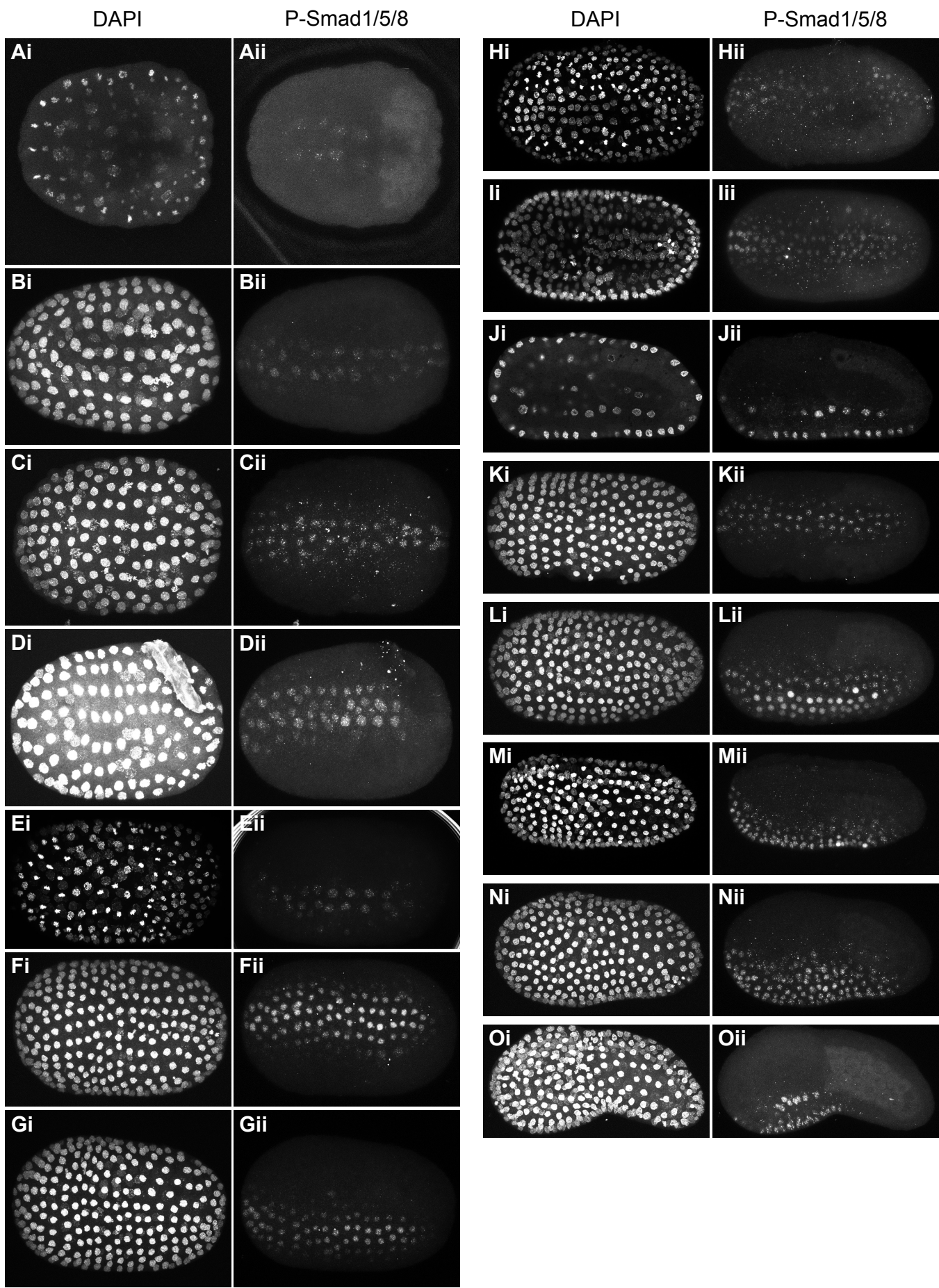
Fig. S4. P-Smad1/5 immunostaining in P. mammillata. Control embryos at various developmental stages were stained with DAPI (i column) and for P-Smad1/5/8 using the #9516 antibody (ii column). The images are maximum intensity projections of confocal z-stacks except J where a confocal section is shown. All embryos are shown with anterior to the left. (A-C) Progressively older gastrulae are shown in ventral views. Note that in Aii only endodermal staining is visible. For the other stages, mostly staining of ventral epidermal midlines is visible. (D-L) Progressively older neurulae are shown in ventral views (D,F,H,I,K) and more or less tilted lateral views with dorsal to the top (E,G,J,L). Ventral epidermis and endoderm staining is visible in Jii. (M-O) Progressively older tailbud stages are shown in lateral views with dorsal to the top. Note that the P-Smad1/5/8 staining was gradually lost from the tail.

Table S1. List of the 1098 genes repressed by BMP signaling in *P. mammillata*. Processing of the *P. mammillata* RNA-seq data from the BioProject PRJNA779382 has been described in (Chowdhury et al., 2022). Here are shown the genes with a negative log2 fold change as calculated by DESeq2 with a p-value<0.05. BvC: BMP4 treatment *vs* control. BvDorso: BMP4 treatment *vs* Dorsomorphin treatment. B+DvC: BMP4+DAPT treatment *vs* control. DvC: DAPT treatment *vs* control.

Click here to download Table S1

Table S2. Expression patterns for a list of the 55 genes regulated by BMP signaling in *P. mammillata*.

Click here to download Table S2

Table S3. List of 68 genes expressed in the palp lineage in *Ciona* or/and *Phallusia*.

Click here to download Table S3

Table S4. Gene identifiers and references. Unique gene identifiers have been retrieved from Aniseed.

Overexpression

Gene name	Gene ID				Reference
Admp	Cirobu.g00004618				Pasini et al., 2006
Noggin	Cirobu.g00003129				Pasini et al., 2006

***Ciona intestinalis* cDNAs**

Gene name	Gene ID	Clone used for ISH	Forward primer	Reverse primer	Reference
Sp6/7/8/9	Cirobu.g00003422	cien70197			Gilchrist et al., 2015
Isl	Cirobu.g00011396				Giuliano et al., 1998
Foxg	Cirobu.g00009441	RT-PCR	AAGACCAGAAACCGTCAACA	GCATCCAATAGTTACCCTTCC	This study.
Foxc	Cirobu.g00012813	cilv050a24			Satou et al., 2002
Celf3/4/5/6	Cirobu.g00007645	citb028e11			Satou et al., 2002
Otx	Cirobu.g00006940				Hudson and Lemaire, 2001
Tfap2-r.b	Cirobu.g00008275	cien223529			Gilchrist et al., 2015
Emx	Cirobu.g00011241	RT-PCR	ATGAATCTGAATAGCCGTTTCGCG	TTACGTCATAGACGCTTGCGTT	This study.
Pou4	Cirobu.g00004616	RT-PCR	ATGTTTACTAACATGCTTGCTCC	TCGATCTCGGATAGGGCAGT	This study.
Msx	Cirobu.g00005203	cign067l18			Satou et al., 2002
Sox14/15/21	Cirobu.g00013989	ciad018l18			Satou et al., 2002

***Phallusia mammillata* cDNAs**

Gene name	Gene ID	Clone used for ISH			Reference
Pou4	Phmamm.g00008914	AHC0AAA33YA19			Coulcher et al., 2020
Celf3/4/5/6	Phmamm.g00007762	AHC0AAA212YP22			Coulcher et al., 2020
Isl	Phmamm.g00000576	McDougall lab			Dardaillon et al., 2020